Aus dem Biomedizinischen Centrum
der Universität München
Lehrstuhl für Molekularbiologie
Vorstand: Prof. Dr. rer. nat. Peter B. Becker

Measurement of S-Adenosyl Methionine in situ

Dissertation
Zum Erwerb des Doktorgrades der Medizin
an der Medizinischen Fakultät der
Ludwig-Maximilians-Universität zu München

Vorgelegt von
Lennart Maximilian Hartmann
Aus Göttingen

2022

Mit Genehmigung der Medizinischen Fakultät der Universität München

Berichterstatter:	Prof. Dr. rer. nat. Axel Imhof
Mitberichterstatter:	Prof. Dr. med. Christian P. Sommerhoff Prof. Dr. rer. nat. Andreas Ladurner
Mitbetreuung durch den promovierten Mitarbeiter:	Dr. rer. nat. Shibojyoti Lahiri
Dekan:	Prof. Dr. med. Thomas Gudermann
Tag der mündlichen Prüfung:	22.12.2022

Eidesstattliche Erklärung

Ich, Lennart Maximilian Hartmann, erkläre hiermit an Eides statt, dass ich die vorliegende Dissertation mit dem Titel

Measurement of S-Adenosyl Methionine in situ

selbständig verfasst, mich außer der angegebenen keiner weiteren Hilfsmittel bedient und alle Erkenntnisse, die aus dem Schrifttum ganz oder annähernd übernommen sind, als solche kenntlich gemacht und nach ihrer Herkunft unter Bezeichnung der Fundstelle einzeln nachgewiesen habe.
Ich erkläre des Weiteren, dass die hier vorgelegte Dissertation nicht in gleicher oder in ähnlicher Form bei einer anderen Stelle zur Erlangung eines akademischen Grades eingereicht wurde.

Ulm, den 04.01.2022

Lennart Maximilian Hartmann

Table of content

Zusammenfassung

Metaboliten sind kleine Moleküle, die viele lebenswichtige Funktionen in Organismen erfüllen. Der Begriff Metabolomik bezeichnet die Erforschung der Metabolite und hat in den letzten Jahren einen deutlichen Zuwachs an Bedeutung erfahren. Dies ist zum einen der Tatsache geschuldet, dass es immer mehr Hinweise für die Unverzichtbarkeit vieler Metabolite in verschiedenen biologischen Abläufen gibt, zum anderen hat der stetige technologische Fortschritt dafür gesorgt, dass die Eigenschaften der Metaboliten sowie deren Dynamik in bis dato unerforschtem Detail untersucht werden können. Zudem sind viele Metaboliten nicht nur in pathophysiologischen Prozessen involviert, sondern besitzen auch ein therapeutisches Potential. Der Metabolit S-Adenosylmethionin (SAM) wird durch das Enzym SAM synthetase produziert und ist der wichtigste Donor einer Methyl-Gruppe in den meisten Organismen. In der Fruchtfliege *Drosophila melanogaster* ist SAM von essentieller Bedeutung nicht nur im Kontext der Entwicklung, sondern auch bei der Regulation der Eingeweide und der Morphologie sowie der Lebensspanne.

In der vorliegenden Arbeit wurden verschiedene Strategien verwendet, um eine Methode zur Messung von SAM in Zellen der *Drosophila melanogaster* zu etablieren. In einem zweiten Schritt wurde untersucht, ob die erhöhte Expression des Enzyms SAM Synthetase eine Auswirkung auf die Menge von SAM in den Zellen besitzt. Die Konzentration von SAM wurde *in vitro*, in lebenden *Drosophila* Zellen sowie in Lysaten der Zellen gemessen. Für die Messungen wurden sowohl auf Fluoreszenz basierende RNA-Aptamere als auch die Massenspektrometrie verwendet.

Erste *in vitro* Ergebnisse zeigten, dass die verwendeten Aptamere eine Bindungsaffinität besitzen, die publizierten Werten entspricht. Es konnten jedoch aufgrund der hohen Autofluoreszenz weder in lebenden *Drosophila* Zellen noch in den Lysaten Veränderungen der SAM-Konzentration mittels der Aptamere gemessen werden. In der Massenspektrometrie zeigten sich ein Anstieg der Konzentration nach Erhöhung der Expression der SAM Synthetase. In einem weiteren Versuch untersuchten wir, ob es dabei eine Veränderung der Konzentration über einen bestimmten Zeitraum gab. Dabei stellte sich heraus, dass die Konzentration 14 sowie 24 Stunden nach Induktion der Expression der SAM Synthetase erhöht war.

Zusammenfassend zeigt die vorliegende Arbeit, dass es einerseits einiger Modifikationen bedarf, um die Veränderungen der SAM-Konzentration mittels RNA-

Aptamere in lebenden *Drosophila* Zellen zuverlässig detektieren zu können. Andererseits resultiert eine erhöhte Expression des Enzyms SAM Synthetase zu einem sich über die Zeit verändernden und mittels Massenspektrometrie messbaren Anstieg der SAM-Konzentration in den Zellen.

Summary

Metabolites are small molecules that execute many essential functions in organisms. The field of studying metabolites, metabolomics, has seen an ever-increasing significance due to constantly evolving technologies which enable improved measurements of metabolites and due to the growing evidence of the importance of these molecules for various biological processes. In addition, not only are metabolites involved in many pathophysiological states and diseases, but they also offer potential therapeutic benefit. S-Adenosyl Methionine (SAM) is a metabolite that is produced by the enzyme SAM synthetase and is the major methyl-donor in most living organisms. SAM has been shown to be a crucial molecule for the organism *Drosophila melanogaster* in the context of developmental lethality, regulation of the midgut, morphology, and lifespan.

In this study, different approaches were used to establish an assay to consistently measure SAM in cells of the model organism *Drosophila*. In a second step, we investigated whether overexpression of the SAM synthetase has any effects on SAM levels. SAM amounts were measured *in vitro*, in live *Drosophila* cells and in lysates by both fluorescence of RNA-based aptamers and Mass Spectrometry (MS).

In vitro experiments showed that the used aptamer possesses the same binding affinity as published in literature. However, due to a high autofluorescence in living *Drosophila* cells and cell lysates no reliable in vivo measurements of SAM could be made using the expressed aptamers. Employing the MS approach, we found an increased SAM level upon induction of expression of the SAM synthetase in *Drosophila* cells. We then investigated whether the overexpression had a time-dependent effect. Our results indicate that SAM levels were increased after 14 and 24 hours of overexpression.

Taken together, the results of this study indicate that some adaptions should be made to enable aptamer-dependent fluorescence imaging of SAM in living cells and that the overexpression of the SAM synthetase in *Drosophila* cells results in increased amounts of SAM in a time-dependent manner detectable by MS.

1. Introduction

1.1. S-Adenosyl Methionine (SAM)

SAM is the major metabolite responsible for many methylation reactions occurring in living organisms (Fontecave et al., 2004). Since its discovery almost 70 years ago (Cantoni, 1953), the biological impact of SAM has been extensively investigated. SAM is produced inside cells when the essential amino acid Methionine reacts with Adenosine triphosphate (ATP). The reaction is catalysed in vivo by the enzyme SAM synthetase. As a result of the methylation reaction SAM is converted to S-Adenosylhomocysteine (SAH), which is subsequently hydrolysed by the SAH hydrolase forming Adenosine and Homocysteine. These reaction products can again be converted to Methionine by Methionine synthetase using either N5methyl Tetrahydrofolate or Betaine as methyl donors (Banerjee und Matthews 1990) thereby forming a metabolic cycle to produce SAM. (Figure 1.1.). Disruption of different reaction steps of this cycle leads to miscellaneous effects. For example, blockage of the SAH hydrolase results in accumulation of SAM due to the feedback inhibition by SAH on most methylation reactions (Chiang et al., 1996). Clinical manifestation of this blockage is demonstrated by decreased blood pressure and an altered gene expression. However, it remains unclear to what extent these effects result from changes of methylation patterns due to inhibition of methylation reactions (Chiang, 1998). These various effects explain why the SAH hydrolase has been the target of many pharmaceutical inhibitors (Hao et al., 2017). Furthermore, changes in SAM metabolism have been linked to both liver diseases and diseases of the neurological spectrum such as depression or other mood disorders, thereby raising the question of not only the pathophysiological role of SAM in these afore mentioned diseases, but also of its therapeutic potential (Lu, 2000). Interestingly, administration of L-Methionine, the predecessor of SAM, was found to elicit an acute schizophrenic episode in patients with chronic schizophrenia in a minor clinical trial (Antun et al., 1971).

A remarkable shared feature of some types of cancer is their absolute requirement for Methionine, also referred to as the “Methionine dependence”. Dietary Methionine restriction in combination with chemotherapy may therefore open new therapeutic options (Cavuoto & Fenech, 2012). Taken together, this data underlines the key role of SAM at both the cellular as well as the organismal level.

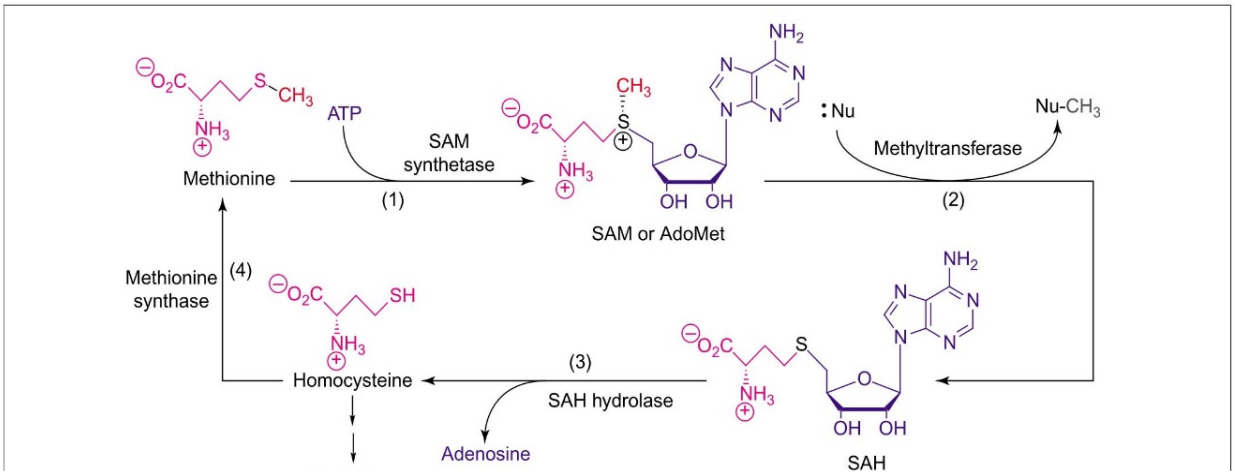

Figure 1.1. The S-Adenosylmethionine (SAM) cycle

Nu represents a nucleophile substrate of methyltransferases. SAM is formed from the reaction of methionine with ATP catalyzed by SAM synthetase (1); methyltransferases catalyze the transfer of the methyl group of SAM to nucleophiles (2); methionine is regenerated from S-adenosylhomocysteine (SAH) by hydrolysis (3) followed by methylation of homocysteine catalyzed by a methionine synthase (4) (reproduced from Fontecave et al., 2004).

1.1.1. Biosynthesis of SAM by the SAM synthetase

Concentration of SAM in mammalian tissue depends on different factors; two of which are the respective organ and the availability of methionine. In liver tissue of rats on a normal diet, SAM was found to range from 50 – 100 nmol/g liver tissue. Most tissues in rats, including brain, lung, intestine and kidney, possess the ability to synthesize SAM (Finkelstein, 1990). The synthesis of SAM is catalysed by an enzyme referred to as SAM synthetase or Methionine Adenosyltransferase (MAT). SAM synthetase is extremely well conserved through evolution in different species. Both mammals and bacteria possess three different isozymes with different tissue-specific expression patterns which form either homo- or heterodimers (Mato et al., 1997). Interestingly, in the fruit fly *Drosophila melanogaster*, this enzyme is encoded by the single *Suppressor of zeste 5 (Su(z)5)* gene (Larsson et al., 1996). To date, according to flybase (https://flybase.org/), this is the only known SAM synthetase gene in *Drosophila melanogaster*. Its significance is demonstrated by the fact that homozygous mutants do not survive early larval stages (Larsson & Rasmuson-Lestander, 1998).

Changes of SAM levels or the SAM synthetase itself also possess clinical relevance. Liver cirrhosis is a potentially deadly disease that presents with various metabolic alterations. Some patients were found to have lower SAM levels in the liver. Notably, it was shown the SAM synthetase is inhibited by free radicals generated during oxidative stress. This inhibition, in combination with reduced synthesis of the antioxidant Glutathione, could be one of the mechanisms leading to reduced SAM levels in liver cirrhosis (Mato et al., 1997). Interestingly, patients with a specific genetic deficiency of the hepatic isozyme of the SAM synthetase usually show persistent hypermethioninemia but no signs of otherwise serious liver disease (Ubagai et al., 1995). The SAM synthetase could also play a major role in the treatment of diseases other than liver cirrhosis. Inhibition of the Methionine Adenosyltransferase II led to apoptotic death of different leukemic cell lines *in vitro* (Jani et al., 2009) and could therefore be a promising target in following clinical trials.

1.1.2. Role of SAM in cellular processes

Methionine and ATP react in the presence of SAM synthetase to produce SAM in the cytosol. This reaction occurs in most cells, but the liver is the major player regarding both the generation and degradation of SAM (Mudd et al., 1980).

SAM participates in three major metabolic pathways: transmethylation, transsulfuration and aminopropylation. Due to this molecular feature, many crucial cellular processes are linked to the SAM cycle. SAM is utilized as the basis for the aminopropylation pathway subsequently leading to the synthesis of polyamines and for the transsulfuration pathway that subsequently leads to the synthesis of Glutathionine (Bottiglieri, 2002). Glutathionine itself is a major cellular antioxidant protecting against reactive oxygen species (Hwang et al., 1992). Polyamines such as Spermidine and Spermine have been shown to be essential for control of cell growth and differentiation (Igarashi & Kashiwagi, 2010). They are also involved in DNA damage repair which may explain some of the clinical effects of the inhibition of SAM metabolism (Lee et al., 2019). Furthermore, Methionine/SAM levels were shown to inhibit autophagy and promote cell growth in yeast mediated by a SAM-dependent methyltransferase, effectively demonstrating the importance of SAM for cellular viability. This is in line with the observation that some cancers show increased uptake of Methionine (Singhal et al., 2008), which is very costly to synthesize endogenously (Sutter et al., 2013).

Impairment of other pathways connected to the SAM cycle can be observed in many diseases. In one of many examples, deletion of the Methylthioadenosine transferase (MTAP), an enzyme which metabolizes the byproduct of polyamine synthesis and leads to eventual regeneration of both Adenosine and Methionine to replenish SAM, often occurs in cancer cells and renders some of them vulnerable to an inhibition of the Methionine Adenosyltransferase II alpha (MAT2A) (Marjon et al., 2016). Downregulation of MTAP has also been associated with tumor progression. In addition, loss of *Mtap* in mice has been shown to cause embryonic lethality (Kadariya et al., 2009).

1.1.3. Relevance of SAM-dependent Methylation

Although SAM is also involved in other cellular processes, most of the 6 – 8 g of the estimated daily SAM production is utilized in methylation reactions (Lu, 2000). Therefore, methylation will be discussed in greater detail. It is important for many essential mechanisms such as brain function and fetal development (Fontecave et al., 2004). The ratio of SAM/SAH is calculated and referred to as the “methylation potential”. It is used to indicate the position of the cellular equilibrium to potentially carry out methylation reactions. A decrease of SAM/SAH in cells reduces the methylation levels (Williams & Schalinske, 2007). Interestingly, a study in Africa showed that a season-associated decrease of the SAM/SAH ratio in women is consistent with lower DNA methylation at specific loci of children conceived during that season (Dominguez-Salas et al., 2013), indicating the potential role of the SAM/SAH ratio in the epigenetic propagation of gene expression patterns across different generations.

In general, various biomolecules such as DNA, RNA, phospholipids, lipids and proteins are substrates of methylation processes (Jani et al., 2009). DNA methylation, usually at the 5-position of cytosine, within the CpG dinucleotide sites of genes, is catalysed by DNA methyltransferases (DNMTs) and is generally associated with gene silencing and transcriptional inactivation (Feinberg & Tycko, 2004). Abnormal DNA methylation as a result of deficiency of the DNMT1 or the methyl-CpG binding protein MBD1 causes abnormal neuronal function and postnatal death (Fan et al., 2001) or decreased neurogenesis and impaired hippocampal function in mice (Zhao et al., 2003).

To further underline its importance, SAM-dependent methylation has also been studied in a clinical background. Methylation of DNA is dysregulated in most cancers (Sun et

al., 2018). Tallying with this, mutations of a specific DNMT are frequently found in acute myeloid leukemia (AML) (Sun et al., 2018). Perturbation of the SAM metabolism either by methionine restriction or by inhibition of SAH hydrolase with subsequent impairment of the methylation potential led to cytotoxicity and induced apoptosis both in established cell lines and patient-derived cells of a specific subtype of leukemia (Barve et al., 2019).

In addition to the DNA itself, proteins bound to DNA are also methylated. The most notable among them being histones. Histones and DNA form chromatin, the main component of the chromosomes of a eukaryotic cell. Histones possess many functions, the dominant of which is the regulation of DNA accessibility and gene expression. Histones are subject to post-translational modifications such as acetylation, phosphorylation and methylation. All histone methyltransferases (HMTs) characterized so far use SAM as the source of a methyl-group which is transferred to the histone (Bannister & Kouzarides, 2011). It is therefore conceivable that methionine metabolic enzymes regulate biological processes such as cell proliferation, development, and the like through controlling genes involved in these processes, whose expression is affected by histone methylation (Liu et al., 2016).

HMTs belong to a group of enzymes, the protein methyltransferases (PMTs), which are responsible for the methylation of not only histones but many other proteins. Emerging evidence suggests that PMTs play pathogenic roles in various diseases such as psychiatric disorders (Tsankova et al., 2007) or cancer (Simon & Lange, 2008). Targeting these enzymes for drug discovery therefore may yield promising results in clinical trials (Copeland et al., 2009).

1.2. Measurement of metabolites

There have been many attempts to establish tools to analyse metabolites due to their biological significance and their possible diagnostic value and therapeutic potential. In order to realise this aim, an entire field of study called metabolomics has evolved. This field describes a holistic approach for comprehensive and systematic identification and quantification of all metabolites (referred to as the metabolome) of a living system such as a cell, tissue or an organism in a given physiological state (Bujak et al., 2015). As metabolites are involved in the execution of almost all cellular processes, changes of the metabolome represent the dynamic perturbations of the genome, the transcriptome (entirety of transcripts) or the proteome (entirety of proteins) of a given biological

system (Bujak et al., 2015). Metabolomics is applied to accomplish a deeper understanding of the pathophysiology of complex diseases such as cancer, diabetes, or cardiovascular disease as well as in the search for new diagnostic and prognostic biomarkers (Bujak et al., 2015; Gowda et al., 2008; Mamas et al., 2011).

Targeted metabolomics involves focusing on measuring the concentrations of a predefined set of metabolites. Establishing a standard curve of the concentration range of the metabolite of interest enables precise quantification of that said metabolite in the process (Johnson et al., 2016). Different techniques are employed to accomplish these goals. In general, measurements are based using nuclear magnetic resonance spectroscopy (NMR) or mass spectrometry (MS) based methods (Markley et al., 2017). NMR probes the chemical characteristics and spatial environment of atomic nuclei whereas MS analyses ionized molecules based on their mass-to-charge-ratio (*m/z*). Materials used to study metabolites contain not only biofluids such as blood and urine but also tissue or even single cells (Zhang et al., 2012; Khamis et al., 2017; Zampieri et al., 2017). However, sole quantification of metabolites does not fully reflect the complex nature of metabolism. Pathway activity, which can be quantified in terms of material flow per unit time (i.e. metabolic flux), must also be taken into account for achieving a complete understanding of the metabolic influence on measured cellular properties (Jang et al., 2018).

A couple of particularly important studies highlight the value of metabolite measurements in the clinical context. It was shown that in human embryonic stem cells, the transition from the naïve to the primed cell state is not only mediated by an enzyme through the control of SAM availability for methylation but also by the metabolic state (Sperber et al., 2015). Another study revealed a key role of serine and glycine metabolism in the survival of glioma cells within ischaemic zones (Kim et al., 2015). These are two of many examples in metabolomic research that have contributed to establishing a clinical link to metabolomics.

1.2.1. RNA aptamers

Recently, specific RNA aptamers have been developed as an additional strategy to detect the presence of certain metabolites and measure their quantities in situ. They are small, single-stranded DNA or RNA molecules of usually 20-100 nucleotides in length. They specifically bind to a defined molecular target via formation of unique three-dimensional structures. Aptamer-based studies are conducted both in basic and

clinical research owing to their versatility as molecular probes (Zhou & Rossi, 2017). Aptamers possess the capability of differentiating between not only conformational isomers (Geiger et al., 1996), but also molecules containing different functional groups (Jenison et al., 1994). In comparison to conventional antibodies, aptamers offer many advantages. Due to their smaller size, aptamers can bind small molecules that are inaccessible for antibodies. Additionally, unlike antibodies, they can be generated to recognize non-immunogenic molecules. Their therapeutic effect can be rapidly reversed by complementary antidote sequences, thereby allowing a fine-tuning system. Furthermore, the generation of aptamers is lower in cost and less likely to be contaminated, and the batch-to-batch variation is dramatically smaller (Zhou & Rossi, 2017). Aptamers, owing to their versatility, have been used in clinical research for the discovery of biomarkers (Phillips et al., 2008) as antagonists (Shum et al., 2013), agonists (McNamara et al., 2008), or delivery agents (Zhou & Rossi, 2014) in several diseases. For example, for the treatment of macular degeneration, one of the most common reasons for blindness in developed countries, aptamer-based therapies are already FDA approved (Drolet et al., 2016).

The RNA aptamer used in this study is referred to as Spinach (Paige et al., 2012; Paige et al., 2011), and its characteristic features as an aptamer are deployed as follows. When the aptamer binds to its target molecule, which is SAM in this study, it undergoes a conformational change, thereby enabling the binding of a specific fluorophore leading to the formation of a SAM-aptamer-fluorophore complex (Figure 1.2.). In an unbound state, the non-specific fluorescence of the fluorophore is minimal. The fluorophore exhibits fluorescence only upon the formation of the aforementioned complex, thereby allowing an estimation of SAM concentration. Spinach can differentiate between highly similar molecules such as ATP and ADP or SAM and SAH. Moreover, Spinach is markedly resistant to photobleaching and does not lead to cytotoxicity, making it a suitable candidate to detect dynamic changes of SAM metabolism over longer periods of time.

In addition to monitoring metabolites, Spinach was also used to track RNA in living cells. It was shown that, upon exertion of cellular stress with sucrose, Spinach-tagged RNA localizes in cytosolic granules, a known cellular reaction to this kind of stress (Paige et al., 2012; Paige et al., 2011). Studies indicated that at least two different intracellular pools of SAM exist; one constantly changing in the cytosol and another

one more stable in the mitochondria (Farooqui et al., 1983). Aptamers may therefore be a powerful tool to further shed light on the spatial distribution of SAM within a cell.

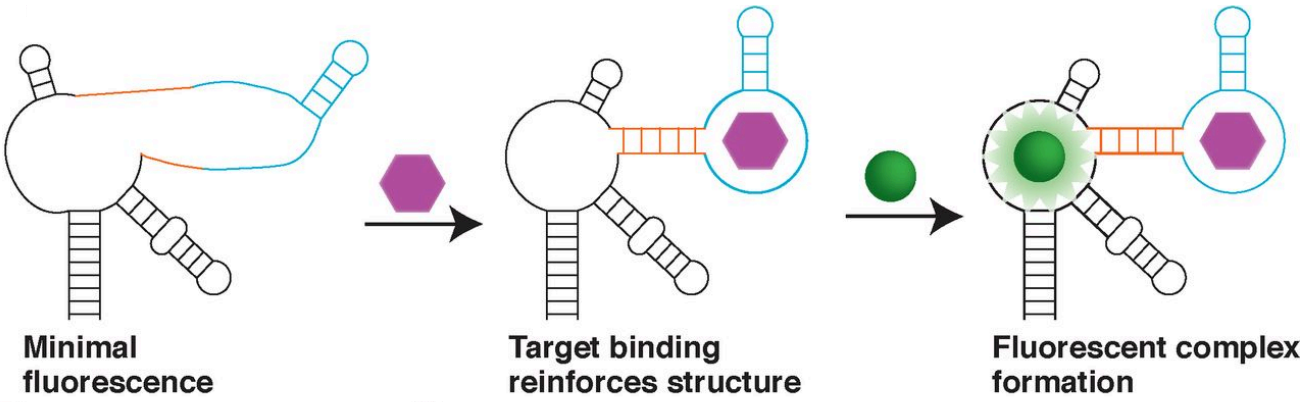

Figure 1.2. Mechanism of Spinach-based fluorescence

The sensor RNA comprises Spinach (black), a transducer (orange), and a target-binding aptamer (blue). Target binding to the aptamer promotes stabilization of the transducer stem, enabling Spinach to fold and activate the fluorescence of the respective fluorophore (green) (adapted from Paige et al. 2012).

1.2.2. Mass spectrometry

Mass spectrometry (MS) is used to reliably identify and quantify molecules such as peptides or metabolites based on their mass-to-charge-ratio (*m/z*). The basic components of a mass spectrometer comprise an ion source, a mass analyser, and an ion detector. Depending on the desired information and the properties of the given sample, the above-mentioned components are combined within an MS instrument. The most commonly used ion sources in these instruments are electron impact ionisation, electrospray ionisation (ESI), desorption electrospray ionisation (DESI) or matrix-assisted laser desorption/ionisation (MALDI). Mass analysers such as the quadrupole (q), the ion trap (IT), the time-of-flight analyser (TOF), and the Fourier transform-ion cyclotron resonance (FT-ICR) analyser separate ions based on their *m/z* employing different physical principles dealing with charged particle dynamics. Ion detection is then usually achieved by electron multipliers or microchannel plates. As soon as an ion strikes their surface, they create a secondary electron cascade resulting in a detectable electron current (Finehout & Lee, 2004; Feng et al., 2008; Henke & Kelleher, 2016; Gundlach-Graham et al., 2018).

Introduction

MS is indispensable for measuring metabolites (Jang et al., 2018). Using MS in metabolomics revealed, for example, that high serum concentrations of the amino acids isoleucine, leucine, valine, tyrosine, and phenylalanine strongly correlate with the risk to develop future diabetes (Wang et al., 2011). Because MS enables the simultaneous measurement of many metabolites, it facilitates the obtainment of a more global metabolic perspective. Limitation of certain nutrients in yeast showed that, in contrast to the change of gene transcripts, the metabolite concentrations were highly sensitive to the limiting nutrient's identity and led to the limitation of growth (Boer et al., 2010). Another work demonstrated the potential use of Diacetylspermine, one member of the polyamine family originally derived from SAM, as a biomarker in the diagnosis of lung cancer (Wikoff et al., 2015). Metabolic flux measurements led to the discovery that, despite its major role as a carbon source to the tricarboxylic acid (TCA) cycle for cancer cells *in vitro* (DeBerardinis et al., 2007), glutamine only minimally contributed to the TCA cycle in lung cancer *in vivo* (Davidson et al., 2016).

In this study, the MALDI-TOF combination was chosen to measure SAM. In MALDI, the sample is co-crystallized within an organic matrix, which is then irradiated with laser pulses. This irradiation leads to excitation of the matrix and ionisation of the analyte resulting in an ejection of the analyte ions to the gas phase (Figure 1.3.). The TOF determines the *m/z* of a selected ion based on the amount of time that passes between the desorption and the moment the ion reaches the detector (Finehout & Lee, 2004).

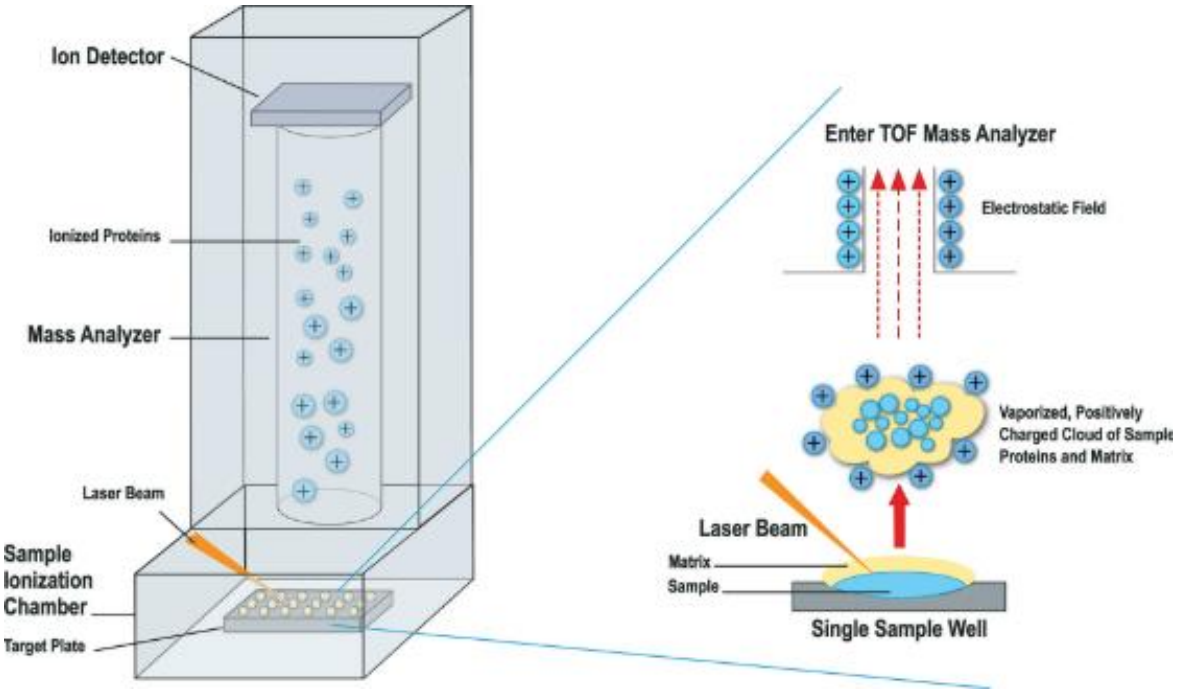

Figure 1.3. Principle of a MALDI TOF mass spectrometer

The spots to be analysed are shot by a laser, desorbing and ionising analytes together with matrix molecules from the target plate. The cloud of ionised molecules is accelerated into the TOF mass analyser, toward a detector. Lighter molecules travel faster, followed by progressively heavier analytes. A mass spectrum is generated, representing the number of ions hitting the detector over time. (adapted from Patel 2015).

1.3. Aim of thesis

SAM is an essential molecule within different organisms and is linked to many crucial mechanisms with far-reaching clinical implications. In *Drosophila melanogaster*, disruption of the Methionine/SAM metabolism affects methylation of histones and results in the loss of viability, which is an additional proof of its essential role. SAM synthetase shows the most significant role in histone methylation among all methionine metabolic genes (Liu et al., 2016). Remarkably, during ageing, systemic SAM levels in flies are increased. However, while a knockdown of SAM synthetase shortens lifespan, a decrease of SAM by overexpression of the Glycine N-methyltransferase (Gnmt) extends lifespan in *Drosophila* (Obata & Miura, 2015). This is further supported by evidence that, under the condition of low amino-acid status, methionine restriction increases lifespan in *Drosophila* (Lee et al., 2014). Establishing an assay to measure the amount of SAM and its varying distribution in different cellular compartments in *Drosophila melanogaster* could therefore give rise to new investigations to further elucidate the manifold roles of SAM metabolism in ageing and disease. If a real-time monitoring of the development of intracellular SAM levels was to be achieved, a connection between the direct effects of the spatial and temporal changes of its concentration and other cellular processes such as repression of gene expression, transcription or translation could be made. To our knowledge, a sensitive, fast, and reliable method to measure intracellular SAM in single *Drosophila melanogaster* cells does not exist to date.

The aim of this thesis was therefore to establish an assay to measure intracellular SAM in a reliable manner. In this work, the model organism *Drosophila melanogaster* was used to develop an assay to detect SAM. To date, no protein-based fluorescence sensors detecting endogenous SAM have been published (Jaffrey, 2018). Therefore, two different techniques were employed to accomplish this goal. First, the described RNA aptamer was utilized to measure SAM from *Drosophila melanogaster* cells *in vitro*. We used a modified version of this aptamer, referred to as Spinach2 (Strack et

al., 2013). In the first step, the *in vitro* binding characteristics of the aptamer were determined. In the next step, cells were subjected to cell lysis and the extracted amount of SAM was measured using the aptamer. Different modification steps were introduced to optimize both the concentration of SAM extracted and the conditions of the measurement. The cells used for this approach comprise standard *Drosophila* L2-4 cells and a *Drosophila* cell line stably transfected with a transgene that allows for the induced expression of SAM-S previously established in our lab. This stable cell line possesses a plasmid coding for the SAM synthetase, which was driven by the copper inducible MT promoter.

Second, a MALDI-MS-based approach was utilized to measure SAM in *Drosophila* cells. The stable cell line was used and, similar to the aptamer-based approach, the expression of the SAM synthetase was induced to detect differences regarding SAM levels between induced cells and untreated control cells. Furthermore, cells at different time points after induction were analysed to assess the dynamic development of SAM levels over a time course of induction of the gene expression.

2. Material and Methods

2.1. Material

2.1.1. Cell lines

Name	Description
Drosophila Schneider L2-4 cells	Clonal isolate from *Drosophila* Schneider S2 cells (Schneider, 1972)
E. coli strain	BL21(DE3) competent *E. coli* (NEB)

2.1.2. Plasmids

Plasmid	Insert	Application
pET 28c	Spinach2 sequence	Generation of Spinach2-RNA molecule (Kanamycin resistance)

pMT	FLAG-HA-Sam-S (N-terminal)	Overexpression of SAM-Synthetase in L2-4 cells (inducible by $CuSO_4$; Hygromycin resistance)

2.1.3. Enzymes

Name	Company
Phusion – High fidelity DNA polymerase	New England Biolabs
T4 DNA ligase	New England Biolabs
Taq polymerase	VWR

2.1.4. Oligonucleotides

Name	Sequence 5´-3´
	In vitro transcription of Spinach2
T7 promotor fw	TAATACGACTCACTATAGGG
Samspin-xho-rev	CTCGAGTGGCGCCCGAAC
	In-Fusion-Cloning of Spinach2
PMT-BSTE-sam-fw	GATAAGGGTTACCGCCCGGATAG
PMT-Xba-sam-rev	ATCCTCTAGATGGCGCCCGA
	RT-PCR of Spinach2
ONLH001 spinach q PCR f	CCGGATAGCTCAGTCGGTAG
ONLH002 spinach q PCR r	CAACCCTTTCGGTTACAAGG
ONLH003 spinach q PCR f	AACGCCAGATGCCTTGTAAC
	CCCGAACAGGGACTTGAAC

ONLH004 spinach q PCR r	

2.1.5. Antibiotics

Name	Company	Stock
Ampicillin	Roth	100 mg/ml (dilution 1:1000)
Hygromycin B	Invitrogen	50 mg/ml
Penicillin/Streptomycin	PAA	10 mg/ml Streptomycin; 10000 Units/ml Penicillin G (dilution 1:100)
Gentamicin	PAA	10 mg/ml (dilution 1:100)

2.1.6. Columns for SPE

Name	Company
Bond Elut PBA, 100mg 1ml	Agilent Technologies

2.1.7. Chemicals

Reagent	Company
1 kb DNA ladder	New England Biolabs
Acetic acid	Sigma Aldrich
Agarose	Bio & Sell
Ammonia	Merck
Ammonium acetate	Merck
$CuSO_4$	Sigma
DFHBI-1T fluorophore	Lucerna
Glycine	VWR
HEPES	VWR
Phenol-Chloroform-Isoamylalkohol	Roth
S-Adenosyl Methionine	NEB/Sigma
Schneider Media	Gibco/Life Technologies
Water	VWR

2.1.8. Equipment

Name	Company
Bioruptor Next Gen	Diagenode
Centrifuge 5424R	Eppendorf
ChemiDocTouch	BIO-RAD
Infinite M1000 Pro	TECAN
rapifleX®	Bruker
Luna II automated cell counter	Biozym
pH 720	InoLab
Rotina 46	Hettich Zentrifugen
Thermomixer C	Eppendorf
Vac Elut 12 and 20 Position Manifold	Agilent
Vortex	Phoenix Instrument

2.1.9. Software

Application	**Software**
Image processing	Power Point Bio-Rad Image Lab Fiji
Office and data analysis	Microsoft Word Microsoft Excel Microsoft PowerPoint GraphPad Prism

2.2. Methods

2.2.1. Microbiology Methods

Plasmid transformation of *E. coli* bacteria

1 µl of plasmid DNA was added to 100 µl chemically competent cells which were thawn on ice. After 60 min incubation, the cell suspension was heat-shocked for 60 s at 42 °C in a water bath followed by incubation on ice for 2 min. All used plasmids carried an ampicillin resistance gene for selection. 200 µl of liquid Luria-Bertani (LB)-medium were added and the cells were incubated for 1 h in a shaking incubator at 37 °C at 850

rpm. Cells were then centrifuged for 3-5 min at 800 g, the supernatant was taken off leaving 300 µl for resuspension. 300 µl of the bacteria were plated on LB-Amp agar plates (ampicillin 100 µg/ml) and incubated o/n at 37 °C. (Method adapted from "plasmid transformation of E.coli bacteria" from PhD thesis, Moritz Völker-Albert, 2017, page: 39).

Luria-Bertani medium

1.0% (w/v) Bacto-Tryptone
1.0% (w/v) NaCl
0.5% (w/v) Bacto-Yeast extract

Growing of bacteria and DNA extraction and purification of plasmid DNA

Single grown colonies were picked and inoculated into 5 ml liquid LB-medium containing the appropriate antibiotics. The cells were incubated o/n in a shaking incubator (Infors Multitron) at 37 °C, 140 rpm for DNA minipreparation. For DNA maxipreparation, 5 ml of grown bacteria in liquid LB-medium were transferred into 500 ml liquid LB-medium with antibiotics for incubation o/n in a shaking incubator at 37 °C, 140 rpm. The subsequent isolation of plasmid DNA was done using Qiagen Plasmid Kits/Macherey-Nagel Kits according to manufacturer's instructions. (Method adapted from "Growing of bacteria and DNA extraction and purification of plasmid DNA" from PhD thesis, Moritz Völker-Albert, 2017, page: 39).

2.2.2. Molecular Biology Methods

Storage of DNA and RNA

Isolated and purified DNA as well as cDNA was stored at -20°C. Isolated RNA was also stored at -20°C in RNase free water. All RNA applications were done with RNase free water, all DNA and RNA experiments were performed in RNase- and DNase free and low-binding tubes (Biozym). (Method adapted from "Storage of DNA and RNA" from PhD thesis, Simone Vollmer, 2016, page 91).

Agarose gel electrophoresis

Agarose gel electrophoresis was performed to separate and distinguish DNA and RNA fragments obtained from restriction digests or PCR reactions.

DNA or RNA fragments migrate with different behaviour according to size and conformation inside an agarose gel. Therefore, the percentage of agarose inside the gel needs to be adapted to the DNA fragments loaded onto the gel. The smaller the fragments for analysis, the higher the percentage of agarose was chosen. Agarose was weighed and dissolved in the appropriate volume of 1x TBE (90 mM Tris, 90 mM Boric acid, 2 mM EDTA) by boiling in the microwave until the solution was completely clear and no small floating particles were visible.
Samples were mixed with 5x loading dye (0.3% (w/v) Orange G, 5 mM EDTA, 50% (v/v) Glycerol) prior to loading onto the gel. To distinguish different fragment lengths, DNA ladders (1 kb, 100 bp, New England Biolabs (NEB)) were used as size standard. Electrophoresis was performed at 50-150 V as determined by the distance of the gel chamber electrodes (4-10 V/cm). Samples were stained with Midori Green Direct (Nippon Genetics) by mixing the samples and DNA ladders with Midori Green Direct at 1:10 (dye:sample) dilution rate. Gels were analysed by radiation with UV light (254-366 nm) and documented by means of a Chemidoc Imaging Touch system (Biorad). For DNA purification from gel, DNA band was excised from the gel with scalpel and purified using Qiagen QIAquick Gel Extraction Kit according to manufacturer's instructions. (Method adapted from "Agarose gel electrophoresis" from PhD thesis, Moritz Völker-Albert, 2017, page: 40)

Polymerase chain reaction

DNA was amplified by polymerase chain reaction (PCR) using Phusion® High-Fidelity DNA Polymerase. This enzyme contains a proofreading function. The following conditions were used:

Template DNA	100 ng plasmid DNA
10x buffer (NEB)	5 µl
Primer fw/rev	0.25 µl each
dNTP mix (10mM each nucleotide, NEB)	1 µl
Phusion® High-Fidelity DNA Polymerase	0.75 µl
ddH_2O	Add to 50 µl

Reaction	**Temperature [°C]**	**Time [s]**

Initial denaturation	95	240	
Denaturation	95	15	25 – 30 cycles
Annealing	56	30	
Elongation	72	30	
Final elongation	72	300	

Reaction products were analyzed using agarose gel electrophoresis as described before and were purified with the GenElute PCR Clean-Up Kit (Sigma Aldrich) after manufacturer's instruction. (Method adapted from "Polymerase chain reaction" from PhD thesis, Simone Vollmer, 2016, page 92).

In vitro transcription

Spinach aptamers were generated using the MEGAScript T7 Transcription Kit according to manufacturer's instructions. RNA was synthesized in 40 µL total volume from 300 ng gel-purified in vitro transcription template. In vitro transcription was performed overnight at 37 °C, followed by 15 min DNase treatment and products were purified using the MEGAclear™ Transcription Clean-Up Kit (Thermo Fischer) according to manufacturer's instructions. Primers for generating in vitro transcription template are listed above. (Method adopted from "Gene knockdown by RNAi" from PhD thesis, Thomas Gerland, 2017, page: 33).

Reverse transcription polymerase chain reaction of uptake of Spinach aptamer in *D. melanogaster* cells

2 µg of RNA per $1x10^6$ cells was added to the cells growing in 25 cm^2 corning flasks. The cells were grown over two days and were harvested as pellets of about 1-1.6 $x10^7$ cells by centrifugation at 800x g for 8 min at 15°C and frozen at -80°. Purification of the cell pellets was performed using the RNeasy Mini Kit (Quiagen) according to manufacturer's instructions. DNase treatment was then performed using the DNase treatment Kit (Roche) according to manufacturer's instructions. cDNA synthesis and reverse transcription polymerase reaction were performed using the SuperScript III First-Strand Synthesis system (Invitrogen) according to manufacturer's instructions.
Analysis of the resulting cDNA was performed by PCR using the following conditions:

Template DNA	2 µl cDNA

10x buffer (NEB)	2.5 µl
Primer fw/rev (10µM)	0.5 µl each
dNTP mix (10mM each nucleotide, NEB)	0.5 µl
Phusion® High-Fidelity DNA Polymerase	0.75 µl
ddH_2O	Add to 25 µl

Reaction	**Temperature [°C]**	**Time [s]**	
Initial denaturation	95	120	
Denaturation	95	30	30 cycles
Annealing	51	30	
Elongation	68	60	
Final elongation	68	300	

Reaction products were analyzed using agarose gel electrophoresis as described before.

2.2.3. Tissue Culture Methods

Cell culture and passaging

D. melanogaster S2-DRSC cells were grown at 26 °C in Schneider's Drosophila medium supplemented with 10 % fetal calf serum and antibiotics (100 units/mL penicillin and 100 µg/mL streptomycin) using 25 cm^2, 75 cm^2 or 175 cm^2 corning flask with 5 mL, 15 mL or 36 mL medium volume respectively. Cells were kept at a density of 0.5-7x10^6 cells/mL. (Method adapted from “Cell culture and passaging” from PhD thesis, Thomas Gerland, 2017, page: 33).

Cell counting and harvesting

Cell density was determined using a LUNA-II cell counter following suppliers’ instructions. For harvesting, cells were resuspended, transferred to falcon tube and spun down at 160 g for 5 min. (Method adapted from “Cell counting and harvesting” from PhD thesis, Thomas Gerland, 2017, page: 33).

Preparation of cell lysates of *D. melanogaster* cells

$7.5x10^7$ cells were harvested and washed once with 1x PBS. Samples were centrifuged at 1000rpm for 6 min at room temperature. The supernatant was discarded and the cell pellet was either flash frozen and stored at -80° or directly used for experiments.
Cell pellets were resuspended in either 4mM Ammonium Acetate buffer (pH 6,7) or 40mM HEPES (pH 7,6) with 125mM KCl and 1mM $MgCl_2$. The sample was then sonicated four times for 10 seconds using the Bioruptor (Diagenode) with pauses of 20 seconds in between and then heated at 80° for 5 min. The sample was then cooled on ice for 10 min and centrifuged at 12000g for 15 min at 4° and the resulting supernatant was used for the fluorescence measurement described below.

Induction of expression of SAM-Synthetase in a stable *D. melanogaster* cell line
Cells of the stable cell line containing a pMT plasmid for overexpression of the SAM-Synthetase were grown in corning flasks and then induced with $CuSO_4$ in a dilution of 1:1000 for two days. $7.5x10^7$ cells were then harvested and centrifuged for 20 min at 1500g at room temperature. Cells were washed twice with 1x PBS and centrifuged for 10 min at 1500g at room temperature. Cell pellets were then either flash frozen and stored at -80° or directly used for experiments.
For evaluating the effect of the time course of the overexpression of the SAM-Synthetase, cells were harvested at the respective time point.

2.2.4. Fluorescence Methods

Cell lysates, respective buffer, RNA, fluorophore and SAM at various concentration were mixed in a well plate and bidest was added to a final well volume of 200 µl. The used concentrations and buffers are listed in the in the context of the respective experiments. The fluorescence of the samples was measured using the Infinite M1000 Pro fluorimeter (TECAN). Fluorescence values of performed experiments were measured at an emission wavelength of 504 nm. The results of the technical replicates were averaged and the fold change in fluorescence (i.e. signal) was calculated as the quotient between RNA + Fluorophore + SAM and RNA + Fluorophore after subtraction of the autofluorescence. The fold change therefore represents the signal. SAM is very unstable at a pH higher than 5 (Laurino & Tawfik, 2017). A higher pH results in the primary degradation product, S-methylthioadenosine and must therefore be avoided during the experiments. To assess the affinity of the Spinach aptamer towards SAM, a

binding curve was generated. The Kd value of the binding curve represents the concentration of SAM where half-maximal fluorescence is reached and therefore reflects the affinity of the aptamer towards SAM (see figure 3.1. B).

Phenylboronic acid (PBA) columns

Previous published studies demonstrated the use of PBA columns when SAM is the target molecule for metabolite measurement (Kirsch et al., 2009). The cell lysate is subjected to the columns in a process called solid phase extraction (SPE). While the other unwanted cellular material flows out of the column, SAM should bind onto the columns. SAM could subsequently be eluted, resulting in enrichment of SAM in the elution and higher resulting fluorescence.

Before SPE, the columns were conditioned five times with 0,3 M acetic acid and five times with 20 mM ammonium acetate (pH 7.5). The primary solution consisting of synthetic SAM or cell lysate was run through the columns, resulting in a flow-through; the columns were then washed twice with 20 mM ammonium acetate (pH 7.5) and three elution steps were performed using 200 µl of 0.3 M acetic acid. To increase the pH of the sample to ensure proper spinach-fluorophore-aptamer complex binding, 3 µl of 25% ammonia was added to the final well volume of 200 µl before fluorescence measurement. Fluorescence was measured and the fold change was calculated afterwards as described above.

2.2.5. Mass Spectrometry Methods

Analysis of the metabolite S-Adenosylmethionine (MALDI-TOF)

For measurement of SAM, cell pellets of cells of interest were generated as described above. Pellets were either flash frozen and stored at -80°C or directly used for further analysis. Cell pellets were resuspended in water (VWR) at a concentration of $15x10^6$ cells/ml. The matrix consisted either of a saturated 2,5-Dihydroxybenzoic acid (DHB) solution in 50% Methanol (MeOH) and 0.1% Formic acid (FA) or a DHB of 30 mg/ml was added to a 50% Methanol (MeOH) and 0.1% Formic acid (FA) solution. Matrix solutions were then sonicated for 20 min at 20°. Resuspended cell pellets and matrix were mixed in a 1:1 dilution and spotted on a target plane. SAM was measured in the reflector mode using positive ion polarity in a RapifleX® (Bruker) MALDI-TOF system. Spectra were acquired (within the range of 280-500 m/z) from the entire spot using the Smart – Complete sample mode with 1000 shots at raster spot using the MS Dried

Droplet laser application. MS2 spectra were obtained using the MSMS small method. Precursor ion at 399.2 m/z was chosen (with an isolation window of ± 2 m/z) for fragmentation with 4000 fragment shots and a laser power boost of 60%. Multiple spectra were accumulated in this mode for the final analysis.

3. Results

3.1. In vitro characterization of Spinach2

3.1.1. Concentration effects of Spinach2 on fluorescence

The RNA aptamer Spinach2 was titrated with the fluorophore DFHBI-1T to determine the optimal RNA concentration for the formation of the RNA-SAM-fluorophore-complex. Three different concentrations of Spinach RNA (0.1 µM, 0.5 µM and 1 µM) were mixed with 1 mM synthetic SAM and 10 µM DFHBI-1T.

Increase in fold change of fluorescence (i.e. signal) was observed with increasing concentration of RNA. (Figure 3.1. A).

This data indicates that within the concentration range of 0.1 and 1 µM, a higher concentration of RNA results in a higher fold change of fluorescence. Thus, staying within the linear range, a concentration of 0.5 µM should be used for the following experiments.

3.1.2. Affinity of Spinach2 towards SAM

Efficient binding of SAM to Spinach2 is important for developing an assay to reliably measure SAM amounts. To determine the affinity of SAM to Spinach2 *in vitro*, we used different concentrations of synthetic SAM that were mixed with 0.48 µM Spinach2-RNA and 10 µM fluorophore.

The measured fluorescence increased with increasing SAM concentration until the reaction reached saturation (at ~ 550 µM) (Figure 3.1. B). An estimate of the dissociation constant (K_d) was made from the half-maximal fluorescence value. Similar to previous reports (Paige et al., 2012), we observed the K_d between Spinach2 and SAM to be 116 µM.

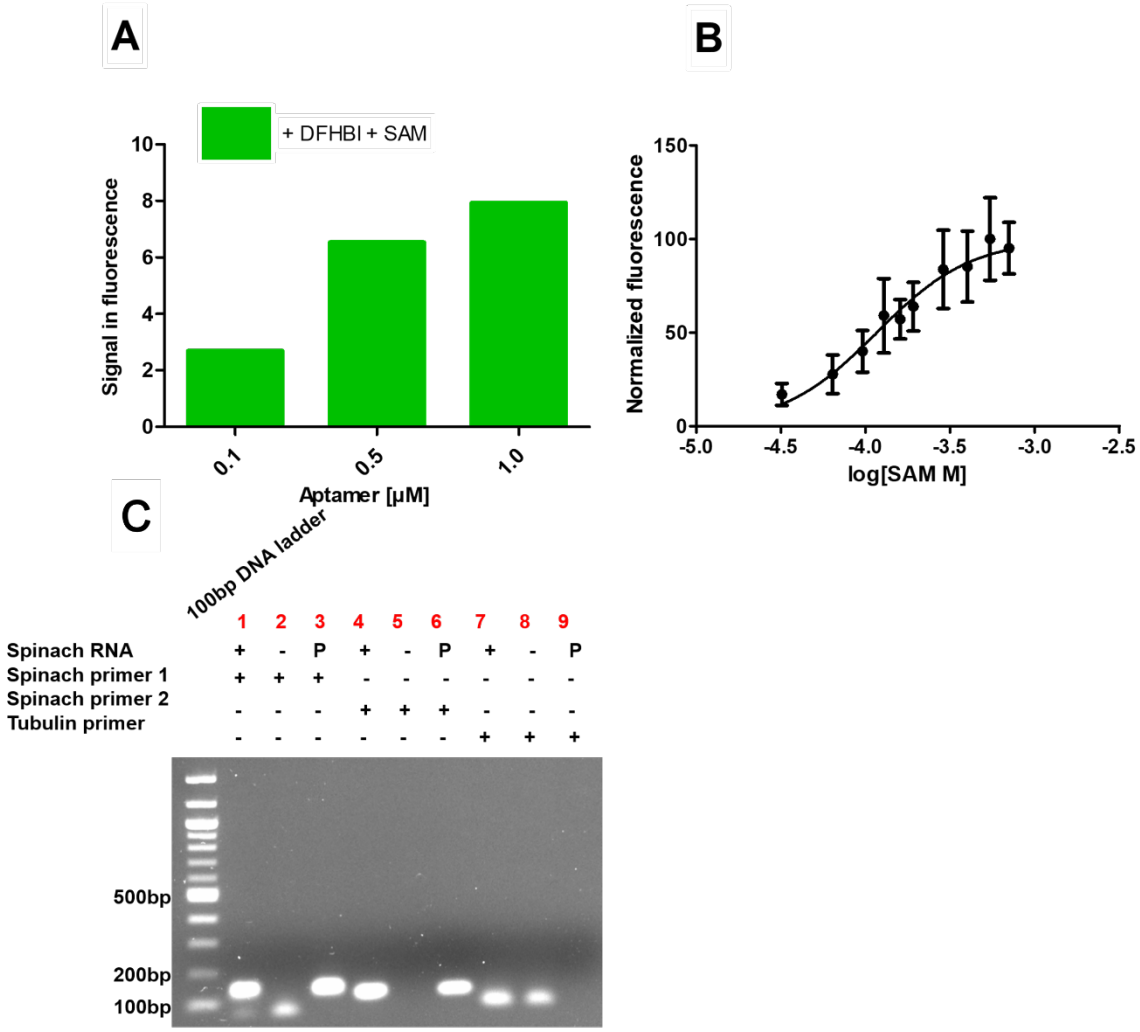

Figure 3.1. *In vitro* characterization of Spinach2 and uptake in *Drosophila* cells

A: Different concentrations of the aptamer were mixed with set concentrations of SAM and DFHBI-1T. Fluorescence was measured, and the respective fold change was calculated.

B: Dose response curve. Different concentrations of SAM were mixed with set concentrations of the aptamer and DFHBI-1T. Fluorescence was measured and normalized (n = 4).

C: L2-4 cells were incubated with the aptamer for two days and harvested. RT-PCR of the cell pellets was performed subsequently. Three different sets were tested, each set consisting of cells incubated with aptamer (lane 1, 4 and 7), cells not incubated with aptamer (lane 2, 5 and 8), and a plasmid coding for the aptamer as a positive control (lane 3, 6 and 9). P = plasmid. Error bars indicate SD.

3.2. Uptake of Spinach2 in *Drosophila* L2-4 cells

After determining the binding characteristics of Spinach2 with synthetic SAM, we proceeded to detect cellular uptake of the RNA aptamer in eukaryotic cells to assess the feasibility of measuring intracellular SAM quantities.

Results

Drosophila L2-4 cells were incubated with 2 µg of aptamer per $1x10^6$ cells for two days. RNA was extracted and subjected to RT-PCR with the two different primer pairs against the aptamer and one primer pair against tubulin as positive control. A plasmid containing the aptamer sequence served as the positive control (P).

Prominent bands were observed at the expected length between 100 and 200 bp (Figure 3.1. C, lane 1 and lane 3), whereas no bands were detected in the controls without Spinach2-RNA (Figure 3.1. C, lane 2 and 5). The bands were similar to those observed in the positive control (Figure 3.3., lane 3 and 6), demonstrating the presence of the aptamer in the cells. The bands appearing below the 100 bp marker are very likely unbound primers (Fig. 3.1. C, lane 1 and 2). As expected, the RT-PCR with primers against the tubulin sequence resulted always in bands regardless of Spinach2-RNA (Figure 3.1. C., lane 7 and 8). Taken together, these findings show that the aptamer was successfully introduced into the cells and that it was not subsequently degraded.

3.3. Measurement of SAM in cell lysates of *Drosophila* cells

It is imperative to have an idea about the cellular quantities of SAM before proceeding to apply Spinach2 for detecting the metabolite inside cells. Therefore, in the next step, cell lysates of *Drosophila* L2-4 cell extracts were used to estimate the cellular quantities of available SAM. Estimation of SAM quantities were thoroughly carried out as described in the following sections.

3.3.1. Induction of SAM synthetase in *Drosophila* L2-4 cells

A stable *Drosophila* L2-4 cell line previously established in the lab was used for inducing SAM generation. This cell line contained a plasmid coding for the enzyme SAM-Synthetase. To test if an induction of expression of the SAM-Synthetase results in a detectably increased concentration of SAM, fluorescence measurements of Spinach2 bound SAM from induced and uninduced cells were compared. 0.2 µM aptamer, 1mM synthetic SAM and 10 µM fluorophore were added to the lysate and fluorescence was measured. Cell lysates were either analysed in an ammonium acetate buffer or a N-(2-Hydroxyethyl)-piperazin-N′-(2-ethansulfonsäure) (HEPES) buffer to determine which buffer is applicable for the aptamer-dependent fluorescence measurement of SAM extracted in cell lysates.

Results

Within the ammonium acetate buffer, addition of synthetic SAM to the lysate increased the signal in both induced and uninduced cells. (Figure 3.2.A).
Similarly, within the HEPES buffer, the signal of fluorophore-bound aptamer compared to fluorophore alone increased upon addition of synthetic SAM in both induced and untreated cells (Figure 3.2.B).
These findings indicate that modifications of the ammonium acetate buffer for the fluorescence measurement are required as only a small increase of fold change upon SAM addition was observed. While these results seem to reinforce the applicability of the HEPES buffer for the aptamer-based fluorescence measurement also in cell lysates, there was not a significant increase in fold change upon induction of the SAM-Synthetase in this buffer. As there is a fold change of 2 without synthetic SAM, this suggests that the HEPES buffer also does extract SAM from the cells in some form during the cell lysis.

3.3.2. Buffer optimization

Addition of cations

It is necessary to optimize the buffer to ensure both hypoosmotic cell lysis to extract intracellular SAM and proper aptamer function for the detection of SAM-based fluorescence. As divalent cations could be crucial for proper aptamer function (Warner et al., 2014), this experiment was performed to assess the effect of their addition to the ammonium acetate buffer without testing cell lysates.
Two different concentrations of ammonium acetate (1.25 mM or 2.5 mM) were used to compare their effect on fluorescence. To do this, 0.48 µM aptamer, 32 µM synthetic SAM and 10 µM fluorophore were added to the cell lysate in presence of 10mM MgCl2 and 150mM KCl. The resulting signal was calculated from the ratio of the fluorescence intensities of SAM and the fluorophore-bound aptamer and the fluorescence of the aptamer in the presence of aptamer only.
In both concentrations of the ammonium acetate buffer, the signal in fluorescence increased upon addition of the ions. (Figure 3.2. C). These observations indicate that the addition of ions to the ammonium acetate buffer is sufficient to increase fluorescence in ammonium acetate buffers.

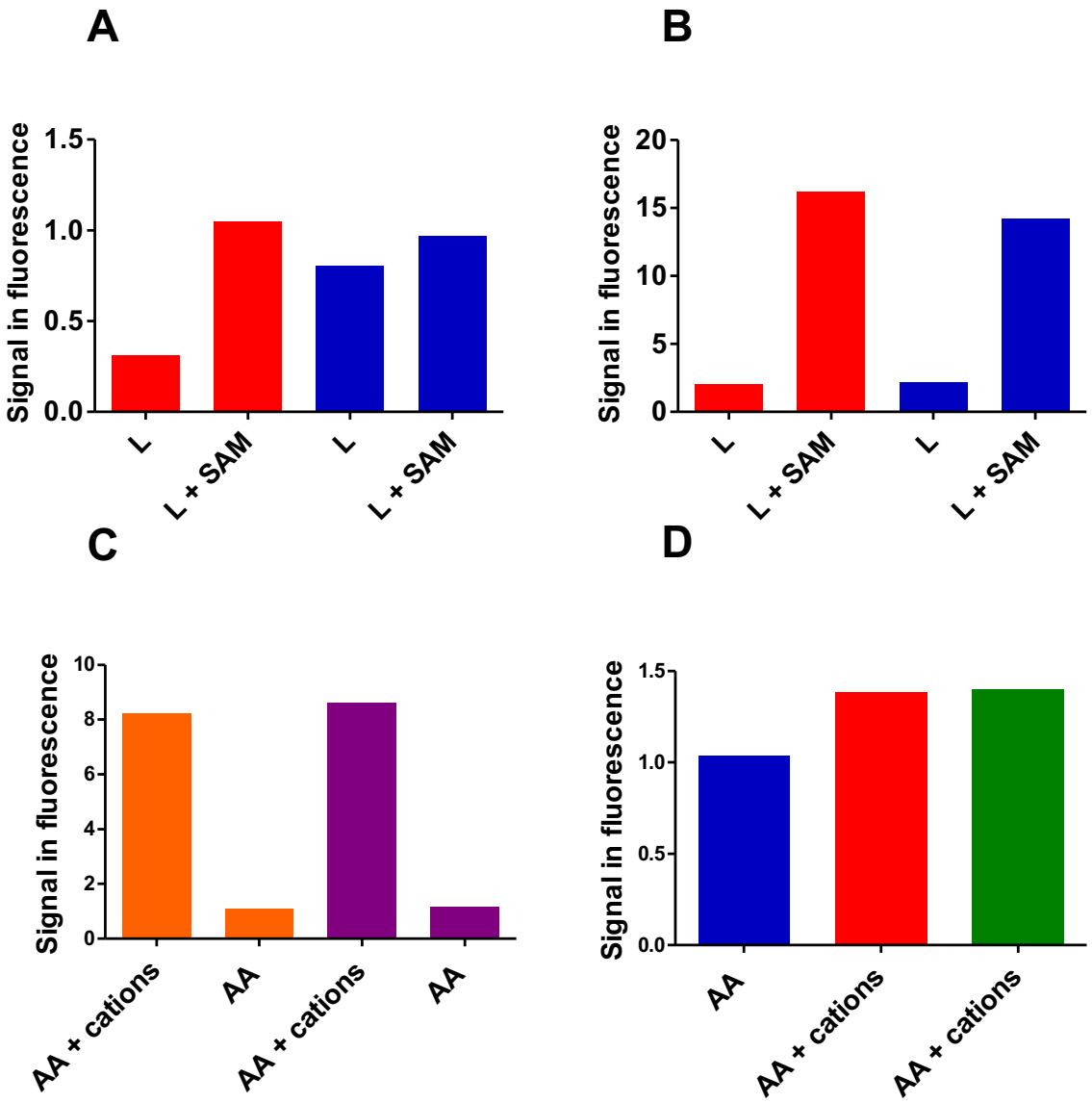

Figure 3.2. Fold change of Spinach dependent fluorescence under different buffer conditions (n = 1)

A and B: Signal in fluorescence upon induction of SAM synthetase in Ammonium acetate buffer (A) or HEPES buffer (B). L2-4 cells were either induced with CuSO4 for two days (red) or remained untreated (blue). The cell lysate was either mixed only with the aptamer and DFHBI-1T or synthetic SAM was added.

C: 10 mM $MgCl_2$ and 150 mM KCl were either added to ammonium acetate buffer of 1,25 mM (orange) or 2,5 mM (purple) or the buffer remained untreated. The different buffers were mixed with the aptamer and DFHBI-1T and SAM.

D: 10 mM MgCl2 and 150 mM KCl (green) or 1 mM MgCl2 and 150 mM KCl (red) were either added to the cell lysate in ammonium acetate buffer or the buffer remained untreated (blue). The different buffers were mixed with the aptamer and DFHBI-1T and SAM.

Comparing different concentrations of added cations in cell lysate in ammonium acetate buffer

After the optimization steps involving the ammonium acetate buffer, this experiment was performed to determine the optimum concentration of the added cations to detect SAM with aptamer-dependent fluorescence in uninduced *Drosophila* L2-4 cell lysates. 10 mM $MgCl_2$ and 150 mM KCl or 1 mM $MgCl_2$ and 125 mM KCl, 0.5 µM aptamer and 10 µM fluorophore were added to the cell lysate.

The addition of ions in the two different concentrations both led to an increase of the fluorescence signal. (Figure 3.2. D).

In the context of previous results, this data shows that, while in absence of the cell lysate, the addition of cations to the ammonia acetate buffer leads to an increase of the fold change in fluorescence. However, the increase in fold change in the presence of the lysate is notably lower, suggesting that the cellular environment may hamper proper buffer function.

3.3.3. Cell lysate dilution

As the addition of ions alone did not improve the results of aptamer-based fluorescence in cell lysates, we hypothesized that the measurement may be hampered by other unspecific cellular material extracted during cell lysis. To test this hypothesis the following dilution experiments with uninduced *Drosophila* L2-4 cells were carried out. The cell lysate was diluted such that it constituted 10% (0.1L), 50% (0.5L) or 100% (L) of a solution, and the different solutions were compared. As an additional positive control, synthetic SAM of 32 µM was tested without any lysate. The signal in fluorescence of the different dilutions of the lysate was lower than that of 32 µM SAM (Figure 3.3. A). This data indicates that dilution alone may not be sufficient to reach similar intensities of fluorescence compared to measuring synthetic SAM.

3.3.4. Enrichment of SAM through phenylboronic acid (PBA) columns

Cell lysate

Initial experiments with cell lysates showed a strong quenching of the SAM fluorescence by cell lysates that could not be overcome by varying the assay conditions. We hypothesized that a partial purification of SAM from the lysate could remove this quenching effect. Previous published studies demonstrated the use of PBA columns when SAM is the target molecule for measurement. The lysate is

subjected to the columns in a process called solid phase extraction (SPE). While the other unwanted cellular material flows out of the column, SAM should bind onto the columns. SAM could subsequently be eluted, resulting in enrichment of SAM in the elution. To test if the use of PBA columns results in enrichment of SAM and hence higher fluorescence intensities, the following experiment was performed. A cell lysate from uninduced *Drosophila* L2-4 cells containing synthetic SAM of 50 µM or 1 mM concentration was subjected to the columns and fluorescence was measured afterwards (Figure 3.3. B). The data suggests that the intracellular SAM concentration within the lysates is lower than 50 µM.

Investigation of SAM degradation during cell lysis

One reason for the low SAM concentration in cell lysates could be the possibility of degradation during lysis. To investigate this, the fluorescence intensity of cell lysates was compared not only to that of untreated synthetic SAM but also to that of synthetic SAM subjected to the cell lysis protocol (cl). Two different approaches were chosen. In the first one, a lysate of uninduced *Drosophila* L2-4 cells was measured, and the solution of synthetic SAM of 100 µM or 1 mM was freshly prepared before measurement of fluorescence. In a second experiment, cell lysates of both induced and uninduced L2-4 cells were used, and the untreated synthetic SAM was prepared at the same time and then stored on ice during the cell lysate protocol. Additionally, to control whether SAM is not bound to the columns or not detected in the environment of the lysate, synthetic SAM (50 µM) was added to cell lysate. Like in previous experiments, the flow through, both wash steps, and three elutions were examined (Figure 3.3. C and D).

Taken together, these findings indicate that that there seems to be no difference in fluorescence between a cell lysate of induced cells or of uninduced cells. The flow through and the wash steps led to the highest fluorescence in both induced and uninduced cells. Signals of synthetic SAM of both concentrations subjected to the cell lysis protocol were lower than those of untreated solutions in the first experiment but similar in the second. Signals of synthetic SAM of both concentrations were lower when stored on ice during the protocol instead of being freshly prepared before the fluorescence measurement. However, synthetic SAM bound to the columns efficiently at a high concentration suggesting that the lack of signal is due to the low intracellular concentrations of SAM rather than SAM degradation during cell lysis.

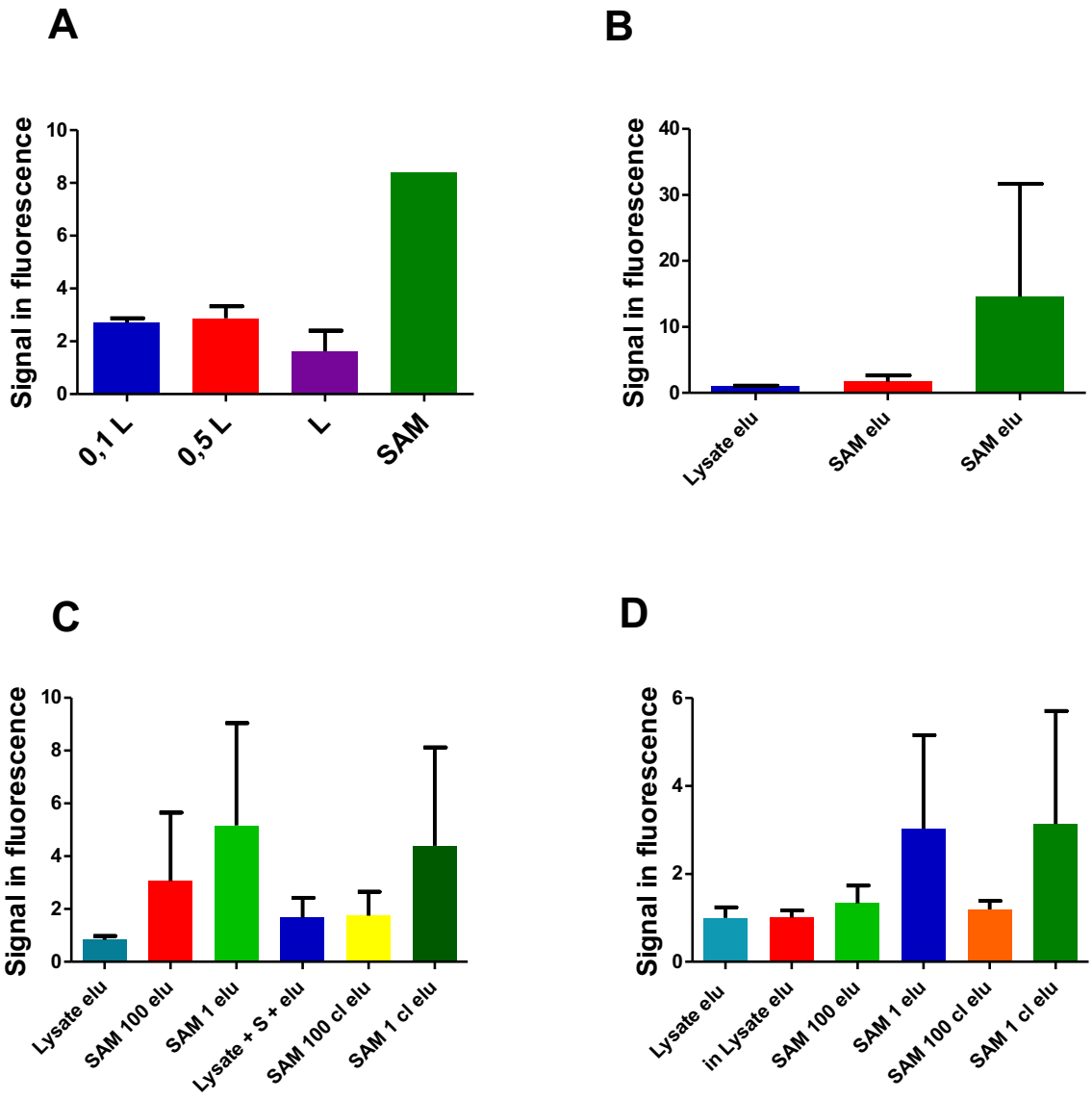

Figure 3.3. Enrichment of SAM via SPE (n = 1)

A: Cell lysates of L2-4 cells were either diluted to half (red) or a tenth (blue) or remained undiluted (purple). The aptamer and DFHBI-1T were added. Fluorescence was measured and fold change was calculated. Synthetic SAM of 32 µM served as a positive control (green

B: Cell lysates of L2-4 cells (green) and synthetic SAM of 50 µM (red) or 1 mM (green) were run through the PBA columns. The flow through, the wash step and the elution were mixed with the aptamer and DFHBI-1T.

C: Synthetic SAM of 50 µM was either added to cell lysates of L2-4 cells (blue) or the cell lysates remained untreated (light blue). Synthetic SAM of 100 µM (yellow) or 1 mM (green) was either subjected to the cell lysis protocol or freshly prepared prior to SPE (red and light green). Cell lysates and SAM were run through the PBA columns. The flow through, the wash

step and the elution were mixed with the aptamer and DFHBI-1T. SAM cl = synthetic SAM subjected to the cell lysis protocol.
D: Cell lysates consisted either of induced (red) or uninduced (light blue) L2-4 cells. Synthetic SAM of 100 µM or 1 mM was either subjected to the cell lysis protocol (orange and green) or stored on ice during SPE (light green and blue). Cell lysates and SAM were run through the PBA columns. The flow through, the wash step and the elution were mixed with the aptamer and DFHBI-1T). Error bars indicate SD.

Influence of pH differences on SAM-dependent fluorescence

Findings of previous experiments revealed high fold changes in fluorescence of 100 µM SAM if prepared directly before being applied to the PBA columns. This also applies if synthetic SAM of 50 µM is added to the lysate directly before applying the lysate to the PBA columns. However, when the 100 µM SAM solution was prepared and stored on ice during the cell lysis protocol, there was only a small fold change in fluorescence whereas there was a large one if the same procedure was done with a 1 mM SAM solution. The synthetic SAM is stored in an acidic solution meaning that, if it is diluted for use in experiments, lower concentrations will result in a higher pH if no further buffer is applied. We hypothesized that, since it had previously been shown SAM is more stable in an acidic environment, a difference in pH could be a possible explanation for this phenomenon. To address this question, SAM of 100 µM and 1 mM was either ran through all steps of the cell lysis protocol (cl) or was kept on ice in the meantime. All four solutions were then subjected to SPE and fluorescence was subsequently measured. Fold change was calculated from the ratio of the fluorescence intensities of SAM and fluorophore-bound aptamer to the fluorescence intensities of fluorophore-bound aptamer alone (Figure 3.4. A).
Taken together, these sets of data indicate that fold changes in fluorescence of 1 mM SAM seem to be higher compared to those of 100 µM regardless of if the SAM solution was kept on ice or was subjected to the cell lysis protocol. In addition, it suggests that subjecting SAM to cell lysis protocol induces degradation and therefore reduced binding to the PBA columns.

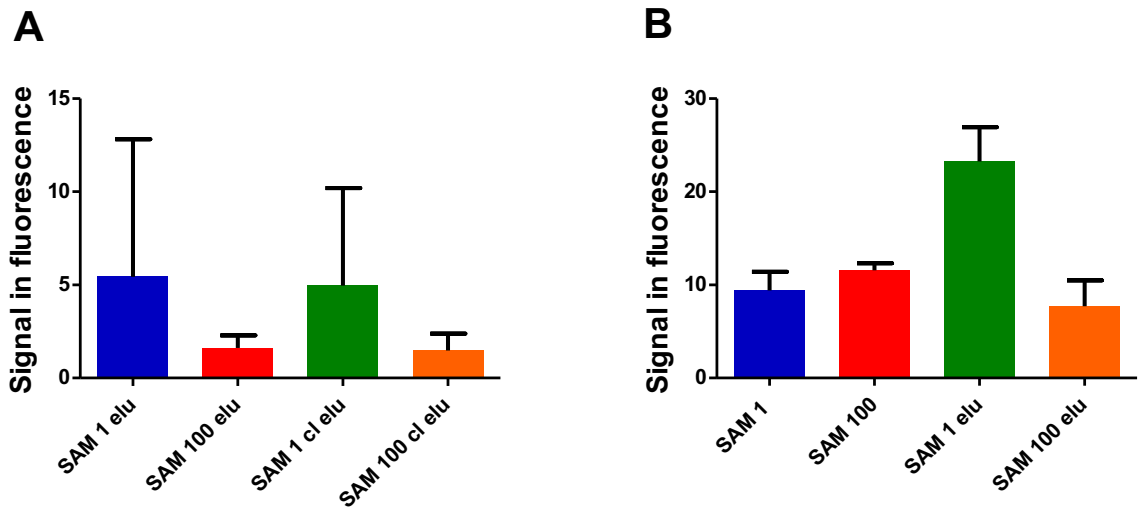

Figure 3.4. Influence of the pH on fold change (A) and fold change before compared to after SPE (B)

A: Synthetic SAM of 100 µM or 1 mM was either stored on ice (blue and red) or subjected to the cell lysis protocol (orange and green). All solutes were then run through the PBA columns. The flow through, the wash step and the elution were mixed with the aptamer and DFHBI-1T. SAM cl = SAM subjected to the cell lysis protocol. (n =1)

B: Synthetic SAM of 100 µM (blue) and 1 mM (red) were mixed with the aptamer and DFHBI-1T and fluorescence was measured. Both solutions were then subjected to the cell lysis protocol. The flow through, the wash step and the elution were mixed with the aptamer and DFHBI-1T (green and orange). (n = 3) Error bars indicate SD.

SAM Recovery experiments

Enrichment of SAM through the application of PBA columns did not result in the expected increase in fold changes of fluorescence intensities from cell lysates. To further examine the ability of the used PBA columns to enrich SAM, the following experiment was performed. Synthetic SAM of two different concentrations (100 µM and 1 mM) was prepared and the fluorescence intensity was measured. The solutions were then applied to the PBA columns, SPE was performed and fluorescence was subsequently measured again. Recovery rate was calculated from the ratio of fold change of elution after SPE to fold change before SPE. As the elutions only account for half of the original solution put into the columns, a recovery rate of two would mean that the concentrations of SAM between the original solution and the elution were equal. Our measurements resulted in a calculated SAM recovery rate of 0.67 at 100

μM and 2.47 at 1 mM (Figure 3.4. B). These findings demonstrate that, compared to a higher concentration, only a small fraction of SAM molecules is recovered at lower concentration. Together with a low intracellular concentration, this could explain the lack of increase of signal in the cell lysate.

3.4. Analysis of SAM in *Drosophila* L2-4 cells by MALDI-TOF MS

As shown above, enrichment of SAM in the cell lysates did not result in a markedly increased fold change of fluorescence. Various factors could account for this finding. The intracellular SAM concentrations of *Drosophila* cells could be relatively too low for the affinity of the aptamer, and the fast degradation processes could furthermore reduce SAM concentrations during the experiments. A different technique was therefore sought to measure SAM in *Drosophila* L2-4 cells. Mass spectrometry (MALDI-TOF) was chosen as it is a sensitive and reliable method to measure small molecules. Theoretical mass of SAM is 399.2 *Da.* and the fragment ions of SAM have masses of 250 *Da.* and 136.2 *Da.* (unpublished data from our group).

MALDI-TOF as a method to measure SAM

To test if the chosen method can reliably detect SAM, first measurements were performed using synthetic SAM. SAM solutions at different concentrations (20 μM, 60 μM and 100 μM) were mixed with a matrix (saturated 2,5-Dihydroxybenzoic acid (DHB) solution in 50% Methanol (MeOH) and 0.1% Formic acid (FA) in a 1:1 (v/v) ratio and were then measured in a Rapiflex MALDI TissueTyper. Measurement of SAM resulted in a peak at the expected 399.2 *m/z* for all the concentrations used but with varying intensities (Figure 3.5.).

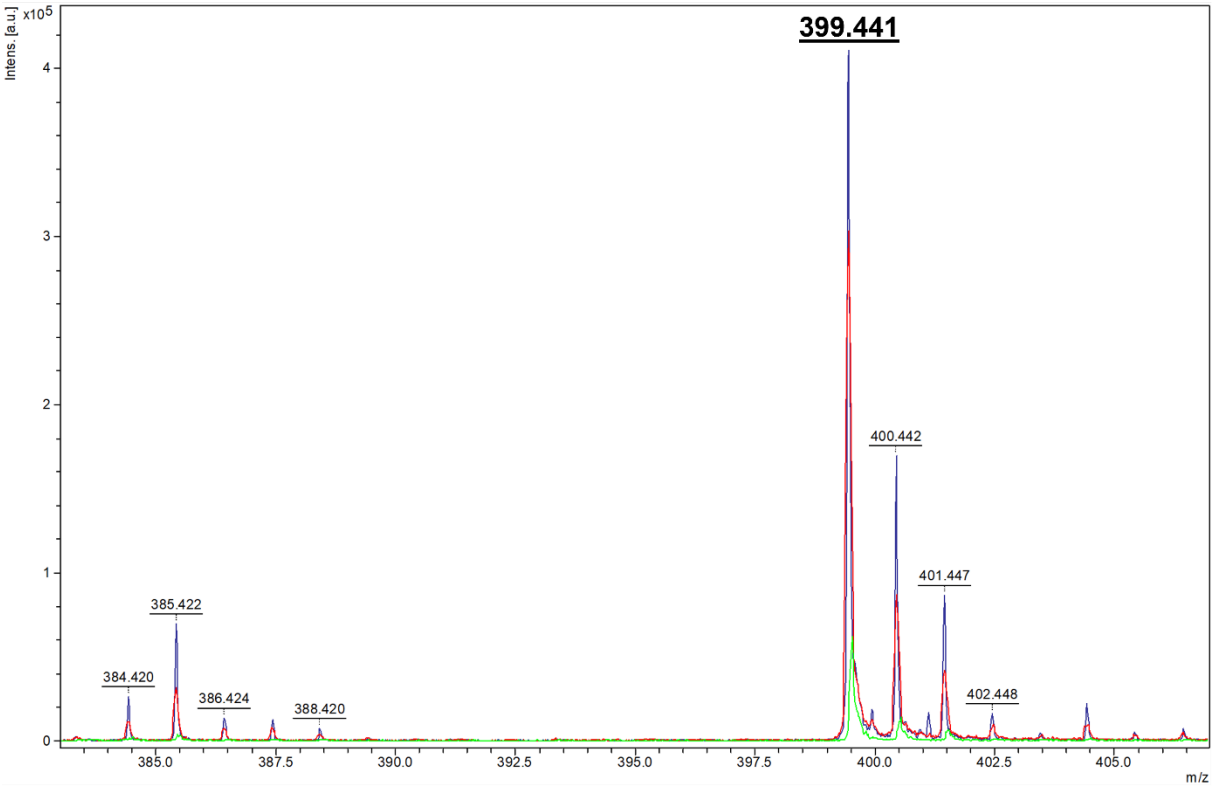

Figure 3.5. Spectra in the SAM mass range of synthetic SAM

Representative ion spectra are shown. Synthetic SAM of 100 (green), 60 (red) and 20 µM (blue) was mixed with a solution of saturated DHB (1:1, v/v). The expected mass of SAM is 399.2 *Da*.

Effect of overexpression of SAM synthetase on SAM levels

After the successful measurement of synthetic SAM, experiments in *Drosophila* cells were performed. To test if changes of SAM levels upon overexpression of the SAM synthetase could be detected by MS, the stable cell line of *Drosophila* L2-4 cells was used. Expression of the plasmid was induced by $CuSO_4$ and uninduced cells were used as a negative control. Additionally, synthetic SAM of different concentrations (20 µM, 60 µM and 100 µM) was either measured alone as a positive control or added to the cells to determine if our experimental setup is applicable for measuring SAM within *Drosophila* cells. Both the cells and synthetic SAM were mixed 1:1 (v/v) with the same DHB matrix described previously and then measured.

Comparison of the spectra between induced und uninduced cells showed that expression of the SAM synthetase led to a peak with higher intensity at the expected *m/z* ratio (Figure 3.6. A), suggesting that there were higher amounts of SAM in the induced cells. To confirm that the peak originated from SAM, further fragmentation of

the peak measured at 399 *m/z* was performed. Fragmentation led to a peak of the fragment ion at the expected 250 *m/z* indicating that the molecule fragmented is indeed representing SAM (Figure 3.6. B). Comparison between the spectra of synthetic SAM alone and synthetic SAM added to induced cells showed that peaks were similar. SAM of 20 µM alone led to the highest peak whereas SAM of 60 µM added to the cells resulted in the highest peak within this combination of SAM and cells (Figure 3.7.A). Comparison between the spectra of synthetic SAM alone and synthetic SAM added to uninduced cells showed that, like in the induced cells, addition of SAM of 60 µM to the uninduced cells led to the highest peak in this combination and that SAM of 20 µM alone exhibited the highest peak overall (Figure 3.7. B). Taken together, these findings indicate that, compared to uninduced cells, overexpression of the SAM synthetase leads to higher amounts of SAM in the corresponding cells. Spectra of fragment ions further confirmed that the peaks indeed originated from SAM. Comparison to spectra of synthetic SAM also serves as additional evidence that the peak at 399 Da originates from cellular SAM.

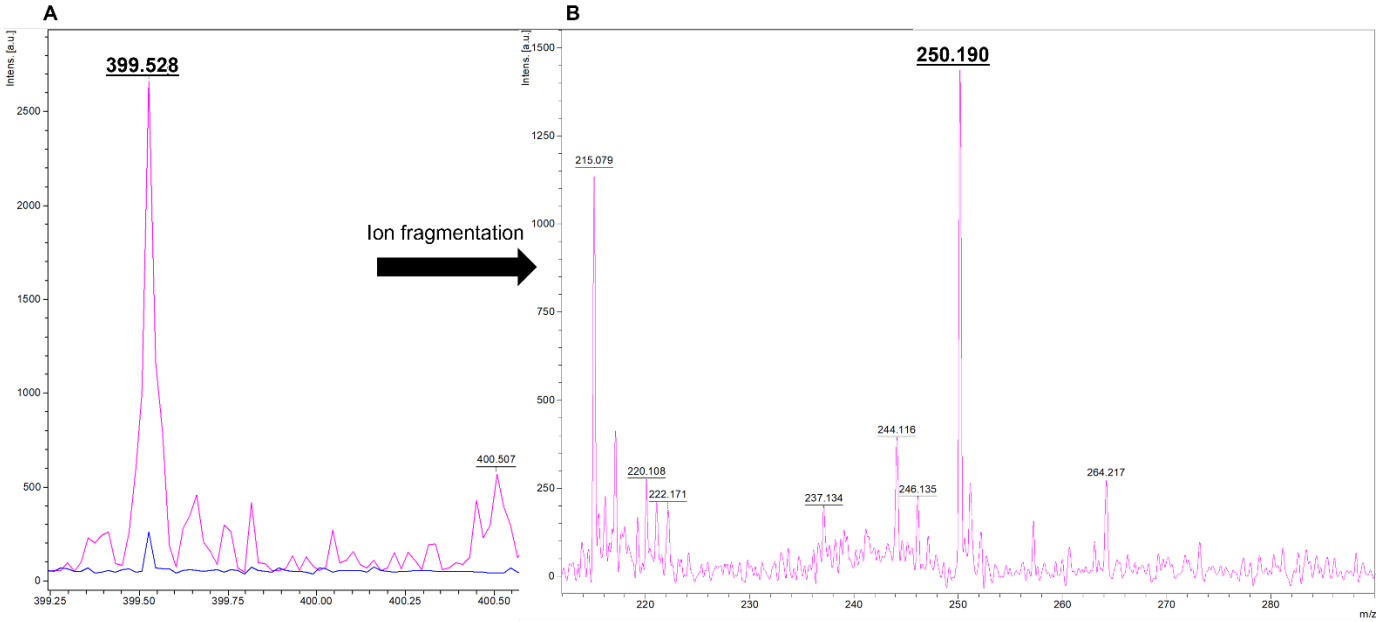

Figure 3.6. Spectra in the SAM mass range of induced and uninduced *Drosophila* cells
Representative ion spectra are shown.
A: L2-4 cells were either induced with $CuSO_4$ for two days (pink) or remained untreated (blue). Cells were mixed with a solution of saturated DHB (1:1, v/v). The expected mass of SAM is 399.2 *Da*.

B: Spectra in the mass range of fragmented SAM of induced *Drosophila* cells. The main product ion of SAM is at 250.0 *m/z* and is thought to correspond to adenosine.

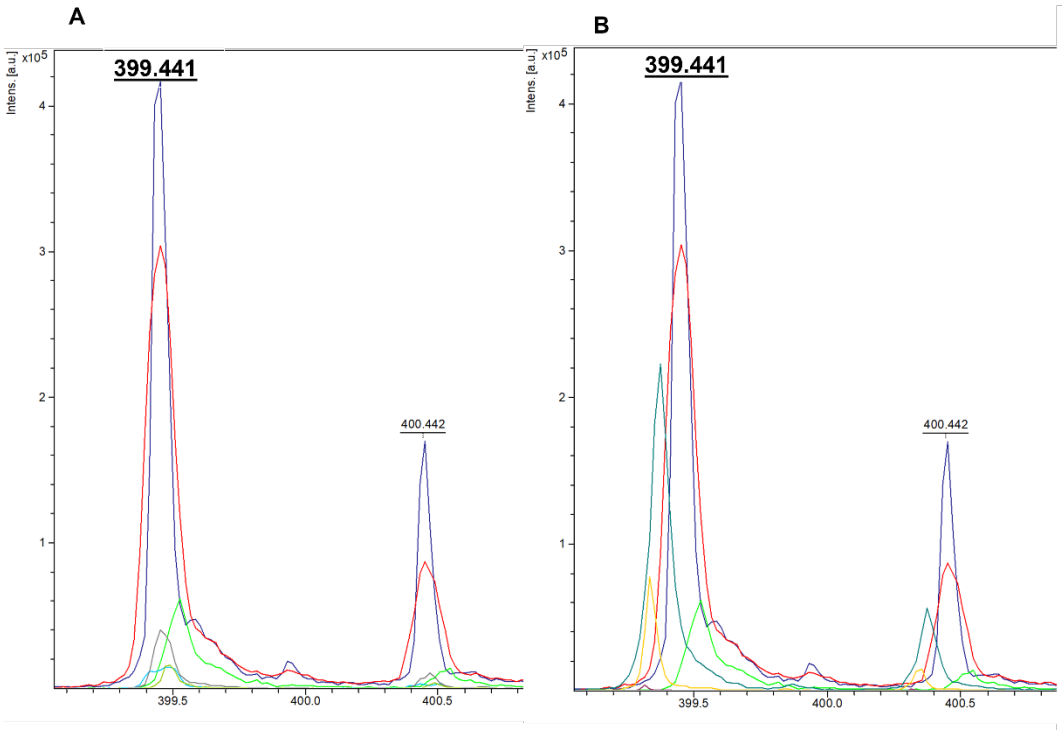

Figure 3.7. Spectra of synthetic SAM and induced (A) and uninduced (B) *Drosophila* cells

Representative ion spectra are shown.

A: Synthetic SAM of 20 (dark blue), 60 (red) or 100 µM (light-green) was either measured alone or added to induced L2-4 cells (light-blue, grey and dark-green). All samples were mixed with a solution of saturated DHB (1:1, v/v). The expected mass of SAM is 399.2 *Da*.

B: Synthetic SAM of 20 (dark blue), 60 (red) or 100 µM (light-green) was either measured alone or added to uninduced L2-4 cells (yellow, blue and brown).

Time course of overexpression of SAM synthetase with saturated matrix

The first experiments using MALDI showed a higher SAM peak in *Drosophila* cells upon induction of SAM synthetase. Subsequent experiments with an unsaturated matrix led to the technical problem that crystallization of the sample appeared only at the outer rim, and the interpretation of the results was therefore inconclusive. To improve the process of crystallization, the ratio between the sample and saturated matrix was changed to 1:1.5 (v/v).

Results

Comparison of the obtained spectra revealed that amounts of SAM increased steadily with time after induction with peaks (399 *m/z*) of highest intensity occurring at 14h and 24h time-points. At 6h of induction, the peak intensity was slightly higher than that of 0h time-point (Figure 3.8.). The spectra of the fragmented ions showed that the peak at 250 *m/z* of 14h of induction was higher than the respective one of 24h of induction. No fragment spectra of 0h and 6h of induction were obtained as they exhibited no signal significantly above the background (Figure 3.9.).

Taken together, these results indicate that the induction of SAM synthetase expression results in higher amounts of SAM compared to the control in a time-dependent manner.

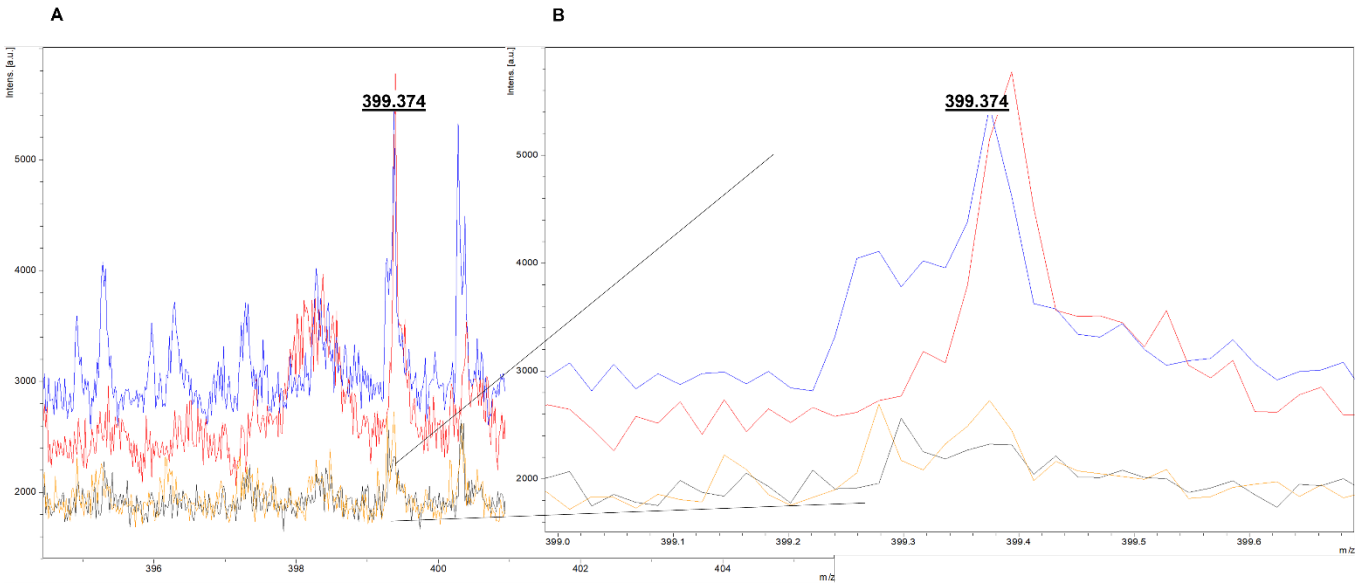

Figure 3.8. Spectra of SAM in induced and uninduced *Drosophila* cells during different time points after induction (A) and zoomed spectra (B)

Representative ion spectra are shown.

A: L2-4 cells were either induced $CuSO_4$ or remained untreated (black). Cells were measured at different time points of induction: 6 hours (orange), 14 hours (red) and 24 hours (blue). Cells were mixed with a solution of saturated DHB (1:1, v/v). The expected mass of SAM is 399.2 *Da.*

B: Zoomed spectra.

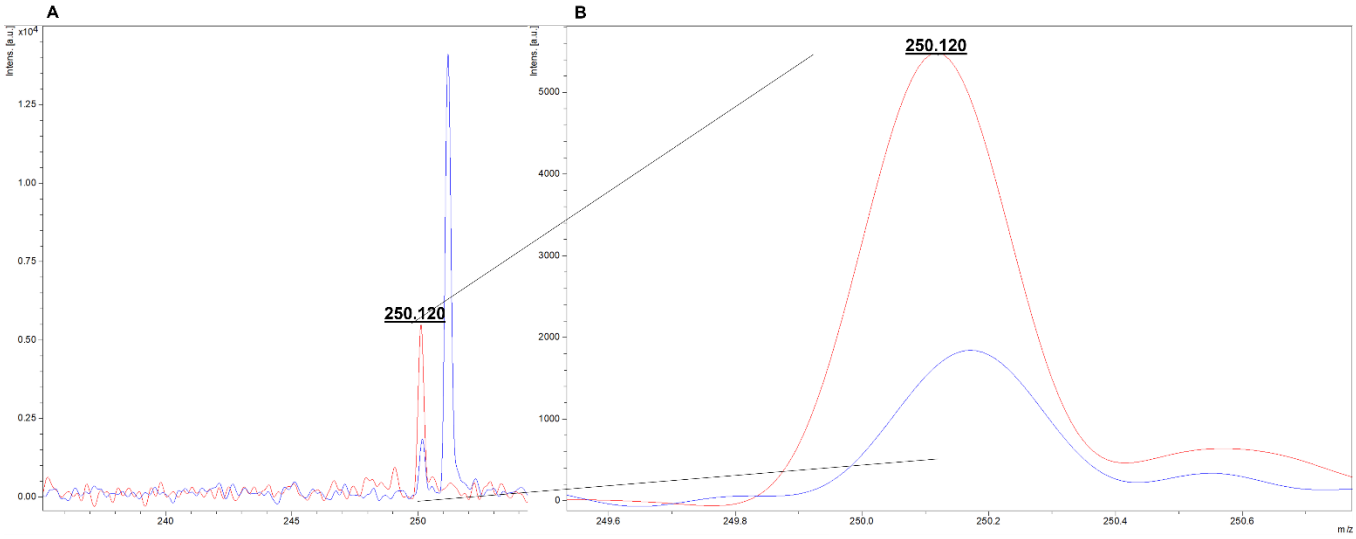

Figure 3.9. Spectra in the mass range of fragmented SAM in induced *Drosophila* cells during different time points after induction (A) and zoomed spectra (B)

Representative ion spectra are shown.

A: L2-4 cells were induced with $CuSO_4$ for 14 hours (red) or 24 hours (blue) Cells were mixed with a solution of saturated DHB (1:1, v/v). The main product ion of SAM is at 250.0 *m/z* and is thought to correspond to adenosine.

B: Zoomed spectra.

4. Discussion

In this study, two different strategies were used to measure SAM in *Drosophila melanogaster* cells. In the first part of this chapter, the use of Spinach-aptamers will be discussed.

4.1. Spinach2-dependent fluorescence assay as a method to measure SAM in *Drosophila* cells

Before the beginning of this work, RNA aptamers had already been shown to be able to provide quantitative measurements of SAM in bacteria (Zhou & Rossi, 2017). In this study, the RNA-based aptamer Spinach2 was expressed in *Drosophila* tissue culture cells with the intention to measure SAM levels *in vivo*. Spinach2 is a modified version of Spinach, which was established as a new aptamer to detect SAM and several other cellular metabolites (Paige et al., 2011; Paige et al., 2012). The modifications of Spinach2 include improved thermal stability and folding in cells (Strack et al., 2013). This family of aptamers was shown to be not only capable of imaging cellular metabolites but also protein expression on a single cell basis (Song et al., 2013). Literature reported a ~20-fold increase in fluorescence upon ligand binding (Strack & Jaffrey, 2013), which should have enabled us to determine SAM levels in eukaryotic cells. However, though we managed to efficiently transfect *Drosophila* cells with RNA aptamers, their high autofluorescence and low intracellular SAM concentration of brightness prevented us from reliably determining the SAM concentration *in vivo*. Using pulsed illumination may improve the experimental setup of imaging live *Drosophila* cells by reducing fluorescence decay as it has been shown in bacteria (Han et al., 2013).

Measurements in cell lysates

Similar to the results in living *Drosophila* cells, experiments with cell lysates did not lead to a strong fluorescent signal over background. Unfortunately, this could neither be improved by buffer optimization nor by a dilution of the lysates for reduction of unspecific signals of cellular material (Figure 3.2. and 3.3.). Application of the PBA columns, which had been used in previous studies (Luippold et al., 1999) to increase the concentration of SAM of the sample was likewise not successful to improve aptamer based fluorescence (Figure 3.3.). Even though it was shown that the background fluorescence of the fluorophore is very low in other eukaryotic cells (Strack

et al., 2013), unspecific activation of the fluorophore by lysate material could be another cause of a low fold change. However, a study using a Spinach-based biosensor to measure a nucleotide in mammalian cell lysates demonstrated that lysates in principle can be used for these aptamer-based fluorescence measurements (Bose et al., 2016). Additionally, application of new fluorophores which have been designed to better suit the setup of fluorimeters or fluorescence microscopy also offers a promising possibility to overcome the problems previously described (Song et al., 2014).

Binding kinetics

Degradation of SAM molecules into SAH could be another major cause for our failure to detect SAM in cells or cellular lysate (Wittmann et al., 2004). However, our study indicates that SAM does not degrade during lysis (Figure 3.3.). SAM decay is also dependent on pH and almost completely ceases at a pH lower than 6 (J L Hoffmann, 1986). We could recapitulate this by aptamer-mediated in vitro measurements (Figure 3.4.). Additionally, accumulating SAH should not impair the measurements as the Spinach-aptamers can discriminate between SAM and SAH (Strack & Jaffrey, 2013). Besides degradation, another problem could be the fact that the intracellular concentration of SAM is too low to be detected adequately by the Spinach2 aptamer. For comparison, in a rat liver, the concentration of SAM was found to be 60 µM (Finkelstein et al., 1982), which is well below the K_d of Spinach2 of around 116 µM (Figure 3.1.). It therefore may be likely that the affinity of the aptamer is not adequate for measurement of intracellular SAM in *Drosophila* cells. Besides optimizing binding kinetics, the use of RNA integrators may offer an alternative in this context as it allows for one target molecule to activate multiple aptamers, thereby amplifying the signal (You et al., 2019).

Future directions

In sum, a relatively low intracellular SAM concentration in combination with rapid degradation of SAM probably accounts for the lack of measurable fluorescence. However, future studies with new developed generations of aptamers or different types of sensors such as riboswitches (Jaffrey, 2018; You et al., 2015) possessing not only elements for enhanced folding properties (Tycowski et al., 2012), but also optimized binding affinities may overcome these shortcomings (Filonov et al., 2014; Song et al., 2017). Application of these “second-generation” fluorogenic RNA-based aptamers

therefore offers a promising possibility of imaging SAM in both live *Drosophila* cells and cell lysates (Karunanayake Mudiyanselage et al., 2019). Most recently it was shown that imaging intracellular SAM in different mammalian cells is not only possible using green-fluorescent aptamers but also red-fluorescent ones, thereby further extending the spectrum of usable fluorophore-aptamer-combinations and indicating that such feats may also be possible to accomplish in *Drosophila* cells in near future (Li et al., 2020).

4.2. MALDI-TOF as a method to measure SAM in *Drosophila* L2-4 cells and the effect of expression of SAM synthetase on cellular SAM levels

Due to the failure of an aptamer-mediated measurement of SAM levels *in vivo*, we decided to measure SAM in *Drosophila* cells and the effect of overexpression of the SAM synthetase on SAM levels using MALDI-TOF MS. MS has been used multiple times to detect and quantify SAM in a rapid and sensitive manner. Employing different MS techniques, the SAM quantity of a variety of biological samples in different organisms is nowadays known. In general, SAM content differs greatly among different tissues. For a better and simplified comparison between the different samples, a few characteristics should be considered.

SAM content in different samples measured by MS

In a mammalian cell, the typical protein content is estimated to be around 100 pg per cell (Budnik et al., 2018). The volume of a human erythrocyte is ~ 100 μm^3 (Frank, A. O., Chuong, C. J. C. and Johnson, R. L., 1979) while the volume of a human lymphocyte is ~ 130 μm^3 (Schmid-Schonbein et al., 1980). In rat kidneys, the tissue content of SAM using MS was found to be about 46 nmol/g weight (Luippold et al., 1999), while it was found to be about 95.6 nmol/g in rat liver (She et al., 1994) and 1443 in rat lung (Stabler & Allen, 2004). Other authors determined the tissue content of SAM in mouse liver and kidney to be 58.3 nmol/g weight and 33.7 nmol/g weight, respectively (Krijt et al., 2009). In ovarian cancer cells, the SAM content ranged from 6 – 20 µg/g protein depending on the cell line used (Iglesias González et al., 2015). In comparison to tissues, SAM both in the cerebrospinal fluid (CSF) and the plasma of humans is in the nanomolar range (Struys et al., 2000; Kirsch et al., 2009). Notably, examination of human urine revealed a level of SAM of 10.7 µmol/l (Ivanov et al., 2016). Evaluation of human blood cells showed that the mean SAM content in human

red blood cells was 3.6 µmol/l (Stabler & Allen, 2004). Another study focussing on intracellular SAM showed that in human lymphocytes, the SAM content was 4.7 nmol per 10^6 cells (Melnyk et al., 2000).

SAM content in Drosophila melanogaster

SAM content and its biological significance in *Drosophila* has been measured and published in different tissues and whole flies, but not in L2-4 cells yet. One study investigated the metabolome of different tissues of *Drosophila* and revealed that the male accessory gland uniquely contained only the decarboxylated form of SAM while other tissues such as testes contained low levels of SAM (Chintapalli et al., 2013). Other authors measured SAM levels of whole flies and demonstrated that attenuating the age-dependent SAM increase has a life-extending effect in *Drosophila* (Obata & Miura, 2015). The same group also showed that SAM regulates stem cell division in *Drosophila* midgut by influencing the protein synthesis (Obata et al., 2018). Others reported that SAM levels in the whole body decreased from 1.7 to 1.2 µmol/g protein to and from 1.5 to 0.9 µmol/g protein in the fat body as a response of the fat body to support repair processes of ablated *Drosophila* imaginal discs and that these repair processes are mediated by connections between the methinonine-SAM and the tryptophan-kynurenine metabolism (Kashio et al., 2016; Kashio & Miura, 2020). Considering that the fat body constantly consists of around 2200 cells (Yongmei Xi, 2015) and assuming the amount of protein to be 100 pg per cell, this would result in an amount of SAM of 0.9 fmol per cell and 0.18 pmol per fat body. In comparison, in our group, unpublished data showed a concentration of endogenous SAM of 1.39 µM in *Drosophila* S2 cells measured by MS. Taken together, few information about the SAM concentration in *Drosophila* exist to date but the concentration seems to differ between the different cell types.

In our study, we measured both synthetic SAM and SAM in *Drosophila* cells. Before evaluating the effect of overexpression of SAM synthetase, we first sought to identify the identity of the MS1 signal. Indeed, using tandem mass spectrometry, we could identify the signal to represent SAM (Figure 3.6. B). In the first step, we examined if there is a difference in SAM levels upon overexpression of the SAM synthetase. Upregulation of this enzyme indeed resulted in an increased peak at the expected *m/z*, and spectra of the fragment ions support the idea that this peak represents SAM (Figure 3.6.). In the second step, the effect of overexpression of the SAM synthetase

on SAM levels in a time-dependent manner was assessed. For this purpose, different time points of overexpression were analysed. We found increased signals after 14 and 24 hours of overexpression but none after 6 hours (Figure 3.8. and 3.9.)

The effect of varying levels of SAM synthetase in *Drosophila*

The regulation of the expression of the SAM synthetase and its effect in *Drosophila melanogaster* have been studied in different contexts. Upregulation of the SAM synthetase was observed in the fat body upon ablation of *Drosophila* imaginal discs as a part of the processes to repair the discs. However, genetic manipulation showed that both up- and downregulation of the SAM synthetase in the fat body impaired disc repair but had no effect on normal wing development (Kashio et al., 2016; Kashio et al., 2017). Correspondingly, knockdown of the SAM synthetase resulted in lethality and defects in wing imaginal discs, but it did not hamper the morphology of adult wings (Liu et al., 2016). Another group was able to bypass the lethality of a knockdown of the SAM synthetase in developmental stages and demonstrated that a knockdown in later stages results in a shortened *Drosophila* lifespan (Obata & Miura, 2015). In our study, an induction of overexpression of SAM synthetase led to an increase of SAM detectable by MS.

Future directions

Quantifying the changes of expression of this enzyme on the molecular level and linking it to quantifiable changes in SAM levels should be the aim of future studies. Furthermore, it should be investigated if overexpression of the SAM synthetase does have effects on the cells regarding multiple biological processes such as ageing, growth, and cell survival. Another future aim should be the examination of the spatial distribution of SAM in *Drosophila* cells. This is also a possible future direction which could be addressed by improved aptamer-dependent imaging of live cells as described in the first chapter.

Discussion

5. References

Antun, F.T., Burnett, G.B., Cooper, A.J., Daly, R.J., Smythies, J.R., and Zealley, A.K. (1971). The Effects of L-Methionine (Without MAOI) in Schizophrenia. Journal of psychiatry Research *8*, 63–71.

Bannister, A.J., and Kouzarides, T. (2011). Regulation of chromatin by histone modifications. Cell research *21*, 381–395.

Barve, A., Vega, A., Shah, P.P., Ghare, S., Casson, L., Wunderlich, M., Siskind, L.J., and Beverly, L.J. (2019). Perturbation of Methionine/S-adenosylmethionine Metabolism as a Novel Vulnerability in MLL Rearranged Leukemia. Cells *8*.

Boer, V.M., Crutchfield, C.A., Bradley, P.H., Botstein, D., and Rabinowitz, J.D. (2010). Growth-limiting intracellular metabolites in yeast growing under diverse nutrient limitations. Molecular Biology of the Cell *21*, 198–211.

Bose, D., Su, Y., Marcus, A., Raulet, D.H., and Hammond, M.C. (2016). An RNA-Based Fluorescent Biosensor for High-Throughput Analysis of the cGAS-cGAMP-STING Pathway. Cell chemical biology *23*, 1539–1549.

Bottiglieri, T. (2002). S-Adenosyl-L-methionine (SAMe): from the bench to the bedside - molecular basis of a pleiotrophic molecule. The American Journal of Clinical Nutrition *76*, 1151–1157.

Budnik, B., Levy, E., Harmange, G., and Slavov, N. (2018). SCoPE-MS: mass spectrometry of single mammalian cells quantifies proteome heterogeneity during cell differentiation. Genome Biology *19*.

Bujak, R., Struck-Lewicka, W., Markuszewski, M.J., and Kaliszan, R. (2015). Metabolomics for laboratory diagnostics. Journal of pharmaceutical and biomedical analysis *113*, 108–120.

Cantoni, G.L. (1953). S-Adenosylmethionine; a new intermediate formed enzymatically from L-methionine and adenosinetriphosphate. Journal of Biological Chemistry.

Cavuoto, P., and Fenech, M.F. (2012). A review of methionine dependency and the role of methionine restriction in cancer growth control and life-span extension. Cancer treatment reviews *38*, 726–736.

References

Chiang, P.K. (1998). Biological Effects of Inhibitors of S-Adenosylhomocysteine Hydrolase. Pharmacology & Therapeutics *77*, 115–134.

Chiang, P.K., Gordon, R.K., Tal, J., Zeng, G.C., Doctor, B.P., Pardhasaradhi, K., and and McCann, P.P. (1996). S-Adenosylmethionine and methylation. The FASEB Journal *10*, 471–480.

Chintapalli, V.R., Al Bratty, M., Korzekwa, D., Watson, D.G., and Dow, J.A.T. (2013). Mapping an atlas of tissue-specific Drosophila melanogaster metabolomes by high resolution mass spectrometry. PloS one *8*.

Copeland, R.A., Solomon, M.E., and Richon, V.M. (2009). Protein methyltransferases as a target class for drug discovery. Nature reviews. Drug discovery *8*, 724–732.

Davidson, S.M., Papagiannakopoulos, T., Olenchock, B.A., Heyman, J.E., Keibler, M.A., Luengo, A., Bauer, M.R., Jha, A.K., O'Brien, J.P., Pierce, K.A., Gui, D.Y., Sullivan, L.B., Wasylenko, T.M., Subbaraj, L., Chin, C.R., Stephanopolous, G., Mott, B.T., Jacks, T., Clish, C.B., and Vander Heiden, M.G. (2016). Environment Impacts the Metabolic Dependencies of Ras-Driven Non-Small Cell Lung Cancer. Cell metabolism *23*, 517–528.

DeBerardinis, R.J., Mancuso, A., Daikhin, E., Nissim, I., Yudkoff, M., Wehrli, S., and Thompson, C.B. (2007). Beyon aerobic glycolysis: transformed cells can engage in glutamine metabolism that exceeds the requirement for protein and nucleotide synthesis. Proceedings of National Academy of Sciences of the United States of America *104*, 19345–19350.

Dominguez-Salas, P., Moore, S.E., Cole, D., da Costa, K.-A., Cox, S.E., Dyer, R.A., Fulford, A.J.C., Innis, S.M., Waterland, R.A., Zeisel, S.H., Prentice, A.M., and Hennig, B.J. (2013). DNA methylation potential: dietary intake and blood concentrations of one-carbon metabolites and cofactors in rural African women. The American Journal of Clinical Nutrition *97*, 1217–1227.

Drolet, D.W., Green, L.S., Gold, L., and Janjic, N. (2016). Fit for the Eye: Aptamers in Ocular Disorders. Nucleic acid therapeutics *26*, 127–146.

Fan, G., Caroline Beard, Richard Z. Chen, Gyorgyi Csankovszki, Yi Sun, Marina Siniaia, Detlev Biniszkiewicz, Brian Bates, Peggy P. Lee, Ralf Kühn, Andreas Trumpp, Chi-Sang Poon, Christopher B. Wilson, and and Rudolf Jaenisch (2001).

References

DNA Hypomethylation Perturbs the Function and Survival of CNS Neurons in Postnatal Animals. The Journal of Neuroscience *21*, 788–797.

Farooqui, J.Z., Lee, H.W., Kim, S., and Paik, W.K. (1983). Studies on compartimentation of S-Adenosyl-L-Methionine in Saccharomyces Cerevisiae and isolated rat hepatocytes. Biochimica et biophysica acta *757*, 342–351.

Feinberg, A.P., and Tycko, B. (2004). The history of cancer epigenetics. Nature reviews Cancer *4*, 143–153.

Feng, X., Liu, X., Luo, Q., and Liu, B.-F. (2008). Mass spectrometry in systems biology: an overview. Mass spectrometry reviews *27*, 635–660.

Filonov, G.S., Moon, J.D., Svensen, N., and Jaffrey, S.R. (2014). Broccoli: rapid selection of an RNA mimic of green fluorescent protein by fluorescence-based selection and directed evolution. Journal of the American Chemical Society *136*, 16299–16308.

Finehout, E.J., and Lee, K.H. (2004). An introduction to mass spectrometry applications in biological research. Biochemistry and Molecular Biology Education *32*, 93–100.

Finkelstein, J.D. (1990). Methionine metabolism in mammals. The Journal of Nutritional Biochemistry *1*, 228–237.

Finkelstein, J.D., Kyle, W.E., Harris, B.J., and and Martin John J. (1982). Methionine Metabolism in Mammals: Concentration of Metabolites in Rat Tissues. The Journal of Nutrition *112*, 1011–1018.

Fontecave, M., Atta, M., and Mulliez, E. (2004). S-adenosylmethionine: nothing goes to waste. Trends in biochemical sciences *29*, 243–249.

Frank, A. O., Chuong, C. J. C. and Johnson, R. L. (1979). A finite-element model of oxygen diffusion in the pulmonary capillaries. Modeling in Physiology, 2036–2043.

Geiger, A., Burgstaller, P., Eltz, H. von der, Roeder, A., and Famulok, M. (1996). RNA aptamers that bind L-arginine with sub-micromolar dissociation constants and high enantioselectivity. Nucleic Acids Research *24*, 1029–1036.

Gowda, G.A.N., Zhang, S., Gu, H., Asiago, V., Shanaiah, N., and Raftery, D. (2008). Metabolomics-based methods for early disease diagnostics. Expert review of molecular diagnostics *8*, 617–633.

References

Gundlach-Graham, A., Hendriks, L., Mehrabi, K., and Günther, D. (2018). Monte Carlo Simulation of Low-Count Signals in Time-of-Flight Mass Spectrometry and Its Application to Single-Particle Detection. Analytical chemistry *90*, 11847–11855.

Han, K.Y., Leslie, B.J., Fei, J., Zhang, J., and Ha, T. (2013). Understanding the photophysics of the spinach-DFHBI RNA aptamer-fluorogen complex to improve live-cell RNA imaging. Journal of the American Chemical Society *135*, 19033–19038.

Hao, W., Li, Y., Shan, Q., Han, T., Li, W., He, S., Zhu, K., Li, Y., Tan, X., and Gu, J. (2017). Characterization of human S-adenosyl-homocysteine hydrolase in vitro and identification of its potential inhibitors. Journal of enzyme inhibition and medicinal chemistry *32*, 1209–1215.

Henke, M.T., and Kelleher, N.L. (2016). Modern mass spectrometry for synthetic biology and structure-based discovery of natural products. Natural product reports *33*, 942–950.

Hwang, C., Sinskey, A.J., and Lodish, H.F. (1992). Oxidized Redox State of Glutathione in the Endoplasmatic Reticulum. Science *257*, 1496–1502.

Igarashi, K., and Kashiwagi, K. (2010). Modulation of cellular function by polyamines. The International Journal of Biochemistry & Cell Biology *42*, 39–51.

Iglesias González, T., Cinti, M., Montes-Bayón, M., La Fernández de Campa, M.R., and Blanco-González, E. (2015). Reversed phase and cation exchange liquid chromatography with spectrophotometric and elemental/molecular mass spectrometric detection for S-adenosyl methionine/S-adenosyl homocysteine ratios as methylation index in cell cultures of ovarian cancer. Journal of chromatography A *1393*, 89–95.

Ivanov, A.V., Virus, E.D., Nikiforova, K.A., Kushlinskii, N.E., Luzyanin, B.P., Maksimova, M.Y., Piradov, M.A., and Kubatiev, A.A. (2016). Capillary electrophoresis and phenylboronic acid solid phase extraction for the determination of S-adenosylmethionine/S-adenosylhomocysteine ratio in human urine. Electrophoresis *37*, 2663–2669.

J L Hoffmann (1986). Chromatographic Analysis of the Chiral and Covalent Instability of S-Adenosyl-L-methionine. Biochemistry *25*, 4444–4449.

References

Jaffrey, S.R. (2018). RNA-Based Fluorescent Biosensors for Detecting Metabolites in vitro and in Living Cells. Advances in pharmacology (San Diego, Calif.) *82*, 187–203.

Jang, C., Chen, L., and Rabinowitz, J.D. (2018). Metabolomics and Isotope Tracing. Cell *173*, 822–837.

Jani, T., Gobejishvili, L., Hote, P., Barve, A., Barve, S., Kharebava, G., Suttles, J., Chen, T., McClain, C., and Barve, S. (2009). Inhibition of methionine adenosyltrasferase II induces FasL expression, Fas-DISC formation and caspase-8-dependent apoptotic death in T leukemic cells. Cell research *19*, 358–369.

Jenison, R.D., Gill, S.C., Pardi, A., and Polisky, B. (1994). High-resolution molecular discrimination by RNA. Sience *263*, 1425–1428.

Johnson, C.H., Ivanisevic, J., and Siuzdak, G. (2016). Metabolomics: beyond biomarkers and towards mechanisms. Nature reviews. Molecular cell biology *17*, 451–459.

Kadariya, Y., Yin, B., Tang, B., Shinton, S.A., Quinlivan, E.P., Hua, X., Klein-Szanto, A., Al-Saleem, T.I., Bassing, C.H., Hardy, R.R., and Kruger, W.D. (2009). Mice heterozygous for germ-line mutations in methylthioadenosine phosphorylase (MTAP) die prematurely of T-cell lymphoma. Cancer research *69*, 5961–5969.

Karunanayake Mudiyanselage, A.P.K.K., Wu, R., Leon-Duque, M.A., Ren, K., and You, M. (2019). "Second-generation" fluorogenic RNA-based sensors. Methods (San Diego, Calif.) *161*, 24–34.

Kashio, S., and Miura, M. (2020). Kynurenine Metabolism in the Fat Body Non-autonomously Regulates Imaginal Disc Repair in Drosophila. iScience *23*, 101738.

Kashio, S., Obata, F., and Miura, M. (2017). How tissue damage MET metabolism: Regulation of the systemic damage response. Fly *11*, 27–36.

Kashio, S., Obata, F., Zhang, L., Katsuyama, T., Chihara, T., and Miura, M. (2016). Tissue nonautonomous effects of fat body methionine metabolism on imaginal disc repair in Drosophila. Proceedings of the National Academy of Sciences of the United States of America *113*, 1835–1840.

Khamis, M.M., Adamko, D.J., and El-Aneed, A. (2017). Mass spectrometric based approaches in urine metabolomics and biomarker discovery. Mass spectrometry reviews *36*, 115–134.

References

Kim, D., Fiske, B.P., Birsoy, K., Freinkman, E., Kami, K., Possemato, R.L., Chudnovsky, Y., Pacold, M.E., Chen, W.W., Cantor, J.R., Shelton, L.M., Gui, D.Y., Kwon, M., Ramkissoon, S.H., Ligon, K.L., Kang, S.W., Snuderl, M., Vander Heiden, M.G., and Sabatini, D.M. (2015). SHMT2 drives glioma cell survival in ischaemia but imposes a dependence on glycine clearance. Nature *520*, 363–367.

Kirsch, S.H., Knapp, J.-P., Geisel, J., Herrmann, W., and Obeid, R. (2009). Simultaneous quantification of S-adenosyl methionine and S-adenosyl homocysteine in human plasma by stable-isotope dilution ultra performance liquid chromatography tandem mass spectrometry. Journal of chromatography. B, Analytical technologies in the biomedical and life sciences *877*, 3865–3870.

Krijt, J., Dutá, A., and Kozich, V. (2009). Determination of S-Adenosylmethionine and S-Adenosylhomocysteine by LC-MS/MS and evaluation of their stability in mice tissues. Journal of chromatography. B, Analytical technologies in the biomedical and life sciences *877*, 2061–2066.

Larsson, J., and Rasmuson-Lestander, A. (1998). Somatic and germline clone analysis in mutants of the S-adenosylmethionine synthetase encoding gene in Drosophila melanogaster. FEBS letters *427*, 119–123.

Larsson, J., Zhang, J., and Rasmuson-Lestander, A. (1996). Mutations in the Drosophila melanogaster Gene encoding S-adenosylmethionine Suppress Position-Effect Variegation. Genetics *143*, 887–896.

Laurino, P., and Tawfik, D.S. (2017). Spontaneous Emergence of S-Adenosylmethionine and the Evolution of Methylation. Angewandte Chemie (International ed. in English) *56*, 343–345.

Lee, B.C., Kaya, A., Ma, S., Kim, G., Gerashchenko, M.V., Yim, S.H., Hu, Z., Harshman, L.G., and Gladyshev, V.N. (2014). Methionine restriction extends lifespan of Drosophila melanogaster under conditions of low amino-acid status. Nature communications *5*, 3592.

Lee, C.-Y., Su, G.-C., Huang, W.-Y., Ko, M.-Y., Yeh, H.-Y., Chang, G.-D., Lin, S.-J., and Chi, P. (2019). Promotion of homology-directed DNA repair by polyamines. Nature communications *10*, 65.

Li, X., Mo, L., Litke, J.L., Dey, S.K., Suter, S.R., and Jaffrey, S.R. (2020). Imaging Intracellular S-Adenosyl Methionine Dynamics in Live Mammalian Cells with a

References

Genetically Encoded Red Fluorescent RNA-Based Sensor. Journal of the American Chemical Society *142*, 14117–14124.

Liu, M., Barnes, V.L., and Pile, L.A. (2016). Disruption of Methionine Metabolism in Drosophila melanogaster Impacts Histone Methylation and Results in Loss of Viability. G3 (Bethesda, Md.) *6*, 121–132.

Lu, S.C. (2000). S-Adenosylmethionine. The International Journal of Biochemistry & Cell Biology *32*, 391–395.

Luippold, G., Delabar, U., Kloor, D., and Mühlbauer, B. (1999). Simultaneous determination of adenosine, S-adenosylhomocysteine and S-adenosylmethionine in biological samples using solid-phase extraction and high-performance lidquid chromatography. Journal of Chromatography B *724*, 231–238.

Mamas, M., Dunn, W.B., Neyses, L., and Goodacre, R. (2011). The role of metabolites and metabolomics in clinically applicable biomarkers of disease. Archives of toxicology *85*, 5–17.

Marjon, K., Cameron, M.J., Quang, P., Clasquin, M.F., Mandley, E., Kunii, K., McVay, M., Choe, S., Kernytsky, A., Gross, S., Konteatis, Z., Murtie, J., Blake, M.L., Travins, J., Dorsch, M., Biller, S.A., and Marks, K.M. (2016). MTAP Deletions in Cancer Create Vulnerability to Targeting of the MAT2A/PRMT5/RIOK1 Axis. Cell reports *15*, 574–587.

Markley, J.L., Brüschweiler, R., Edison, A.S., Eghbalnia, H.R., Powers, R., Raftery, D., and Wishart, D.S. (2017). The future of NMR-based metabolomics. Current opinion in biotechnology *43*, 34–40.

Mato, J.M., Alvarez, L., Ortiz, P., and Pajares, M.A. (1997). S-Adenosylmethionine Synthesis: Molecular Mechanisms and Clinical Implications. Pharmacology & Therapeutics *73*, 265–280.

McNamara, J.O., Kolonias, D., Pastor, F., Mittler, R.S., Chen, L., Giangrande, P.H., Sullenger, B., and Gilboa, E. (2008). Multivalent 4-1BB binding aptamers costimulate CD8+ T cells and inhibit tumor growth in mice. The Journal of clinical investigation *118*, 376–386.

Melnyk, S., Pogribna, M., Pogribny, I.P., Yi, P., and James, S.J. (2000). Measurement of Plasma and Intracellular S-Adenosylmethionine and S-

References

Adenosylhomocysteine Utilizing Coulometric Electrochemical Detection: Alterations with Plasma Homocysteine and Pyridoxal 5′-Phosphate Concentrations. Clinical chemistry *46*, 265–272.

Mudd, S.H., Ebert, M.H., and Scriver, C.R. (1980). Labile Methyl Group Balances in the Human: The Role of Sarcosine. Metabolism *29*, 707–720.

Obata, F., and Miura, M. (2015). Enhancing S-adenosyl-methionine catabolism extends Drosophila lifespan. Nature communications *6*, 8332.

Obata, F., Tsuda-Sakurai, K., Yamazaki, T., Nishio, R., Nishimura, K., Kimura, M., Funakoshi, M., and Miura, M. (2018). Nutritional Control of Stem Cell Division through S-Adenosylmethionine in Drosophila Intestine. Developmental cell *44*, 741-751.

Paige, J.S., Nguyen-Duc, T., Song, W., and Jaffrey, S.R. (2012). Fluorescence imaging of cellular metabolites with RNA. Science (New York, N.Y.) *335*, 1194.

Paige, J.S., Wu, K.Y., and Jaffrey, S.R. (2011). RNA mimics of green fluorescent protein. Science (New York, N.Y.) *333*, 642–646.

Patel R. MALDI-TOF MS for the diagnosis of infectious diseases. Clin Chem. 2015 Jan;61(1):100-11. doi: 10.1373/clinchem.2014.221770. Epub 2014 Oct 2. PMID: 25278500.

Phillips, J.A., Lopez-Colon, D., Zhu, Z., Xu, Y., and Tan, W. (2008). Applications of aptamers in cancer cell biology. Analytica chimica acta *621*, 101–108.

Schmid-Schonbein, G.W., Shih, Y.Y., and Chien, S. (1980). Morphometry of human leukocytes. Blood *56*, 866–875.

Schneider, I. (1972). Cell lines derived from late embryonic stages of Drosophila melanogaster. Journal of embryology and experimental morphology *27*, 353–365.

She, Q.-B., Nagao, I., Hayakawa, T., and Tsuge, H. (1994). A simple HPLC method for the determination of S-Adenosylmethionine and S-Adenosylhomocysteine in rat tissues: the effect of Vitamin B6 deficiency on these conctentrations in rat liver *205*, 1748–1754.

Shum, K.-T., Zhou, J., and Rossi, J.J. (2013). Aptamer-based therapeutics: new approaches to combat human viral diseases. Pharmaceuticals (Basel, Switzerland) *6*, 1507–1542.

References

Simon, J.A., and Lange, C.A. (2008). Roles of the EZH2 histone methyltransferase in cancer epigenetics. Mutation research *647*, 21–29.

Singhal, T., Narayanan, T.K., Jain, V., Mukherjee, J., and Mantil, J. (2008). 11C-L-methionine positron emission tomography in the clinical management of cerebral gliomas. Molecular imaging and biology *10*, 1–18.

Song, W., Filonov, G.S., Kim, H., Hirsch, M., Li, X., Moon, J.D., and Jaffrey, S.R. (2017). Imaging RNA polymerase III transcription using a photostable RNA-fluorophore complex. Nature chemical biology *13*, 1187–1194.

Song, W., Strack, R.L., and Jaffrey, S.R. (2013). Imaging bacterial protein expression using genetically encoded RNA sensors. Nature methods *10*, 873–875.

Song, W., Strack, R.L., Svensen, N., and Jaffrey, S.R. (2014). Plug-and-play fluorophores extend the spectral properties of Spinach. Journal of the American Chemical Society *136*, 1198–1201.

Sperber, H., Mathieu, J., Wang, Y., Ferreccio, A., Hesson, J., Xu, Z., Fischer, K.A., Devi, A., Detraux, D., Gu, H., Battle, S.L., Showalter, M., Valensisi, C., Bielas, J.H., Ericson, N.G., Margaretha, L., Robitaille, A.M., Margineantu, D., Fiehn, O., Hockenbery, D., Blau, C.A., Raftery, D., Margolin, A.A., Hawkins, R.D., Moon, R.T., Ware, C.B., and Ruohola-Baker, H. (2015). The metabolome regulates the epigenetic landscape during naive-to-primed human embryonic stem cell transition. Nature cell biology *17*, 1523–1535.

Stabler, S.P., and Allen, R.H. (2004). Quantification of serum and urinary S-adenosylmethionine and S-adenosylhomocysteine by stable-isotope-dilution liquid chromatography-mass spectrometry. Clinical chemistry *50*, 365–372.

Strack, R.L., Disney, M.D., and Jaffrey, S.R. (2013). A superfolding Spinach2 reveals the dynamic nature of trinucleotide repeat-containing RNA. Nature methods *10*, 1219–1224.

Strack, R.L., and Jaffrey, S.R. (2013). New approaches for sensing metabolites and proteins in live cells using RNA. Current opinion in chemical biology *17*, 651–655.

Struys, E.A., Jansen, E.E., Meer, K. de, and Jakobs, C. (2000). Determination of S-Adenosylmethionine and S-Adenosylhomocysteine in Plasma and Cerebrospinal

References

Fluid by Stable-Isotope Dilution Tandem Mass Spectrometry. Clinical chemistry *46*, 1650–1656.

Sun, Y., Chen, B.-R., and Deshpande, A. (2018). Epigenetic Regulators in the Development, Maintenance, and Therapeutic Targeting of Acute Myeloid Leukemia. Frontiers in oncology *8*, 41.

Sutter, B.M., Wu, X., Laxman, S., and Tu, B.P. (2013). Methionine inhibits autophagy and promotes growth by inducing the SAM-responsive methylation of PP2A. Cell *154*, 403–415.

Tsankova, N., Renthal, W., Kumar, A., and Nestler, E.J. (2007). Epigenetic regulation in psychiatric disorders. Nature reviews. Neuroscience *8*, 355–367.

Tycowski, K.T., Shu, M.-D., Borah, S., Shi, M., and Steitz, J.A. (2012). Conservation of a triple-helix-forming RNA stability element in noncoding and genomic RNAs of diverse viruses. Cell reports *2*, 26–32.

Ubagai, T., Lei, K.J., Huang, S., Mudd, S.H., Levy, H.L., and Chou, J.Y. (1995). Molecular mechanisms of an inborn error of methionine pathway. Methionine adenosyltransferase deficiency. The Journal of clinical investigation *96*, 1943–1947.

Wang, T.J., Larson, M.G., Vasan, R.S., Cheng, S., Rhee, E.P., McCabe, E., Lewis, G.D., Fox, C.S., Jacques, P.F., Fernandez, C., O'Donnell, C.J., Carr, S.A., Mootha, V.K., Florez, J.C., Souza, A., Melander, O., Clish, C.B., and Gerszten, R.E. (2011). Metabolite profiles and the risk of developing diabetes. Nature medicine *17*, 448–453.

Warner, K.D., Chen, M.C., Song, W., Strack, R.L., Thorn, A., Jaffrey, S.R., and Ferré-D'Amaré, A.R. (2014). Structural basis for activity of highly efficient RNA mimics of green fluorescent protein. Nature structural & molecular biology *21*, 658–663.

Wikoff, W.R., Hanash, S., DeFelice, B., Miyamoto, S., Barnett, M., Zhao, Y., Goodman, G., Feng, Z., Gandara, D., Fiehn, O., and Taguchi, A. (2015). Diacetylspermine Is a Novel Prediagnostic Serum Biomarker for Non-Small-Cell Lung Cancer and Has Additive Performance With Pro-Surfactant Protein B. Journal of clinical oncology official journal of the American Society of Clinical Oncology *33*, 3880–3886.

References

Williams, K.T., and Schalinske, K.L. (2007). New Insights into the Regulation of Methyl Group and Homocysteine Metabolism. The Journal of Nutrition *137*, 311–314.

Wittmann, C., Krömer, J.O., Kiefer, P., Binz, T., and Heinzle, E. (2004). Impact of the cold shock phenomenon on quantification of intracellular metabolites in bacteria. Analytical biochemistry *327*, 135–139.

Yongmei Xi, Y.Z. (2015). Fat Body Development and its Function in Energy Storage and Nutrient Sensing in Drosophila melanogaster. Journal of Tissue Science & Engineering *06*.

You, M., Litke, J.L., and Jaffrey, S.R. (2015). Imaging metabolite dynamics in living cells using a Spinach-based riboswitch. Proceedings of the National Academy of Sciences of the United States of America *112*, E2756-65.

You, M., Litke, J.L., Wu, R., and Jaffrey, S.R. (2019). Detection of Low-Abundance Metabolites in Live Cells Using an RNA Integrator. Cell chemical biology *26*, 471-481.

Zampieri, M., Sekar, K., Zamboni, N., and Sauer, U. (2017). Frontiers of high-throughput metabolomics. Current opinion in chemical biology *36*, 15–23.

Zhang, A., Sun, H., and Wang, X. (2012). Serum metabolomics as a novel diagnostic approach for disease: a systematic review. Analytical and bioanalytical chemistry *404*, 1239–1245.

Zhao, Z., Tetsuya Ueba, Brian R. Christie, Basam Barkho, Michael J. McConnell, Kinichi Nakashima, Edward S. Lein, Brennan D. Eadie, Andrew R. Willhoite, Alysson R. Muotri, Robert G. Summers, Jerold Chun, Kuo-Fen Lee, and and Fred H. Gage (2003). Mice lacking methyl-CpG binding protein 1 have deficits in adult neurogenesis and hippocampal function. Proceedings of the National Academy of Sciences of the United States of America *100*, 6777–6782.

Zhou, J., and Rossi, J. (2017). Aptamers as targeted therapeutics: current potential and challenges. Nature reviews. Drug discovery *16*, 181–202.

Zhou, J., and Rossi, J.J. (2014). Cell-type-specific, Aptamer-functionalized Agents for Targeted Disease Therapy. Molecular therapy. Nucleic acids *3*, e169.

6. Abbreviations

DHB	Dihydroxybenzoic Acid
DFHBI-1T	(5Z)-5-[(3,5-Difluoro-4-hydroxyphenyl)methylene]-3,5-dihydro-2-methyl-3-(2,2,2-trifluoroethyl) -4H-imidazol-4-one
FA	Formic Acid
MeOH	Methanol
MS	Mass Spectrometry
RNA	Ribonucleic Acid
SAH	S-Adenosylhomocysteine
SAM	S-Adenosylmethinonine
SD	Standard Deviation
SPE	Solid Phase Extraction

7. Acknowledgements

Zuallererst möchte ich mich bei Axel Imhof für die Möglichkeit bedanken, dass ich mir dieses spannende Forschungsthema in seinem Labor erarbeiten sowie die ersten Schritte in die experimentelle Forschung wagen durfte. Lieber Axel, vielen Dank für Deine kontinuierliche Betreuung und Deine vielen Ratschläge! Deine Kreativität sowie Dein Enthusiasmus für die Forschung waren sehr ansteckend, und ich habe sehr viel während meiner Zeit im Labor gelernt!

Weiterhin bedanken möchte ich mich bei Peter Becker, dass ich an seinem Institut forschen und von der damit einhergehenden und beeindruckenden Infrastruktur desselben profitieren konnte. Ich habe dabei neben der täglichen Arbeit im Labor viel über das Wesen der Wissenschaft sowie die Rolle eines Wissenschaftlers und die zwingende Notwendigkeit einer stets kritischen Reflexion aller Tatsachen und Erkenntnisse gegenüber verinnerlicht.

Ganz besonders möchte ich auch Irene Vetter und Shibojyoti Lahiri danken, die mir während meiner Zeit im Labor und auch im Anschluss beim Verfassen dieser Arbeit stets tatkräftig zur Seite standen und mich bei allen Fragen jeglicher Natur immer unterstützt haben. Liebe Irene, lieber Shibo, ich werde die Zeit im Labor mit euch vermissen!

Mein Dank gilt zudem Simone Vollmer, Elisa Oberbeckmann und Moritz Völker-Albert für die Unterstützung bei der Analyse der Daten sowie dem Verfassen dieser Arbeit. Liebe Simone, darüber hinaus bin ich gespannt, was wir noch in der Welt der Ophthalmologie gemeinsam erleben werden!

Ebenso danken möchte ich allen Mitgliedern der Imhof group für die Unterstützung sowie das Feedback während unserer Laborbesprechungen. Dank euch bereichert nun der Begriff „breakthrough sience“ meinen Wortschatz! Mein Dank gilt auch allen Kollegen am Institut sowie am BMC, die mich in welcher Form auch immer bei meinen Experimenten unterstützt haben. Es hat Spaß gemacht, mit euch zu arbeiten!

Darüber hinaus möchte ich mich auch bei allen Verantwortlichen des Förderungsprogrammes für Forschung und Lehre der LMU München ("FöFoLe") für die fachliche sowie finanzielle Unterstützung bedanken.

Ein weiteres Dankeschön gebührt meinen Freunden sowie meiner Verwandtschaft, die mich auf allen Höhen und Tiefen während dieser Reise begleitet haben und mir dabei stets den Rücken gestärkt haben. Dabei möchte ich Clara Eichberger sowie Johanna und Jonathan Schindler gesondert hervorheben. Liebe Clara, liebe Johanna und lieber Jonathan, ich konnte mich zu jedem Zeitpunkt auf eure Hilfe verlassen und bin euch dafür mehr als dankbar!

Zuletzt möchte ich mich noch bei meinen Eltern bedanken, ohne deren Unterstützung ich nicht bis zu diesem Punkt gekommen wäre.